UNIVERSITAT POLITÈCNICA DE CATALUNYA
BARCELONATECH
Escola Superior d'Enginyeries Industrial,
Aeroespacial i Audiovisual de Terrassa

Design and thermomechanical study of the case of a solid rocket motor of small dimensions

Document:
Annexes

Author:
Jan Canet Vidal

Director / Co-director:
Dr. Juan Carlos Cante Terán
Dr. David Roca Cazorla

Degree:
Bachelor's degree in Aerospace Technology Engineering

Examination session:
Spring, 2022

BACHELOR FINAL THESIS

Appendix A

Thesis planning

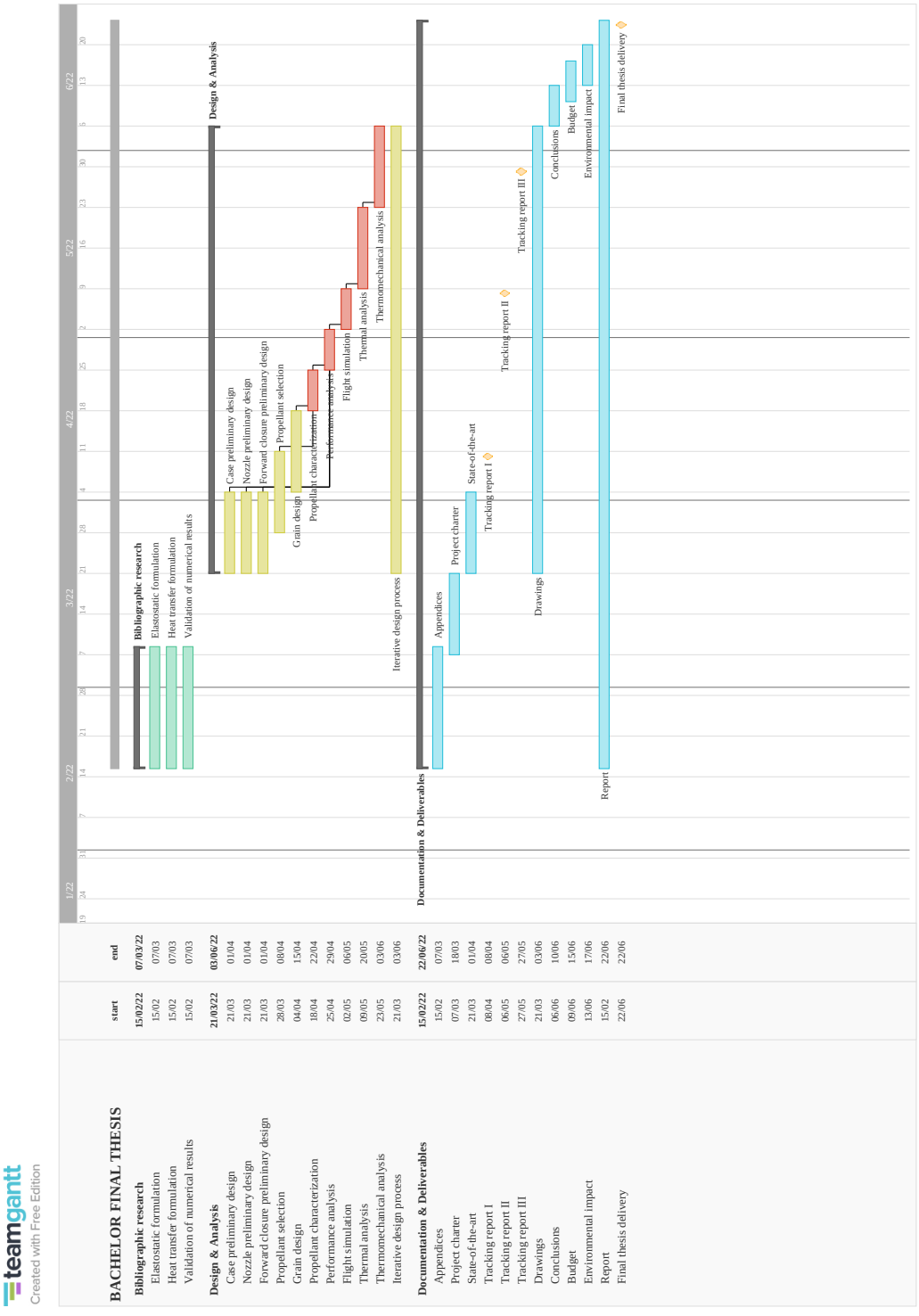

Appendix B

Heat transfer equations in cylindrical coordinates

Conduction

In order to derive the differential equation of conduction heat transfer in cylindrical coordinates, one must first define an infinitesimal control volume (CV) of the elemental surroundings of an arbitrary point in space. Then, the heat fluxes entering and leaving the CV must be drawn as well, as shown in figure B.1. In this case, the control volume is static.

The surfaces and volume of the elemental CV are the following:

$$\begin{aligned} dV &= rdrd\theta dz & S_\theta &= drdz \\ S_r &= rd\theta dz & S_z &= rdrd\theta \end{aligned} \tag{B.1}$$

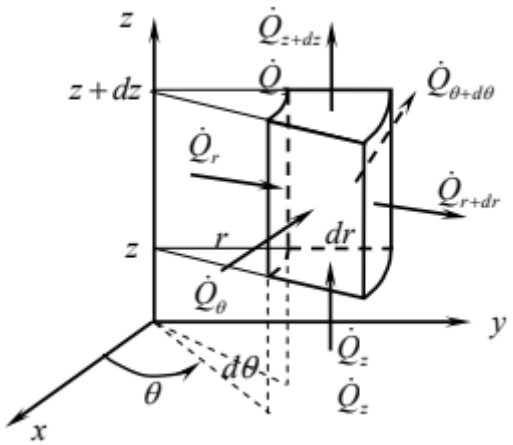

Figure B.1: Cylindrical elemental control volume and its respective heat fluxes (Source: [22]).

Since in conduction heat transfer there is no fluid flow, the internal energy variation of the CV must be equal to the heat flow

$$\frac{\partial}{\partial t}\int_V \rho u \, dV = \dot{Q} \tag{B.2}$$

From the left hand side (LHS) of equation (B.2), the integral can be omitted, since the volume is infinitesimal, the volume differential can get out of the derivative, since it is not time dependent (the volume does not change) and, the density does not depend on time either.

$$\frac{\partial}{\partial t}\int_V \rho u \; dV = \frac{\partial(\rho u dV)}{\partial t} = \rho\frac{\partial u}{\partial t}dV$$

From the right hand side (RHS) of equation (B.2), the heat flux can be expressed as the sum of the different heat flux components in each direction.

$$\dot{Q} = \dot{Q}_r - \dot{Q}_{r+dr} + \dot{Q}_\theta - \dot{Q}_{\theta+d\theta} + \dot{Q}_z - \dot{Q}_{z+dz} + \dot{q}_v dV$$

where $\dot{q}_v dV$ stands for the internal sources of heat.

The substitution of this two expressions yields

$$\rho\frac{\partial u}{\partial t}dV = \dot{Q}_r - \dot{Q}_{r+dr} + \dot{Q}_\theta - \dot{Q}_{\theta+d\theta} + \dot{Q}_z - \dot{Q}_{z+dz} + \dot{q}_v dV \tag{B.3}$$

By substituting the following expressions in the above equation, one obtains equation (B.4).

$$\begin{cases} \dot{Q}_{r+dr} = \dot{Q}_r + \dfrac{\partial \dot{Q}_r}{\partial r}dr \\ \dot{Q}_{\theta+d\theta} = \dot{Q}_\theta + \dfrac{\partial \dot{Q}_\theta}{\partial \theta}d\theta \\ \dot{Q}_{z+dz} = \dot{Q}_z + \dfrac{\partial \dot{Q}_z}{\partial z}dz \end{cases}$$

$$\rho\frac{\partial u}{\partial t}dV = -\frac{\partial \dot{Q}_r}{\partial r}dr - \frac{\partial \dot{Q}_\theta}{\partial \theta}d\theta - \frac{\partial \dot{Q}_z}{\partial z}dz + \dot{q}_v dV \tag{B.4}$$

Introducing the Fourier Law (equation (B.5)) and the expression that relates internal energy with temperature (equation (B.6)), one obtains equation (B.7).

$$\text{(Fourier Law)} \quad \begin{cases} \dot{Q}_r = -\lambda\dfrac{\partial T}{\partial r}S_r \\ \dot{Q}_\theta = -\lambda\dfrac{1}{r}\dfrac{\partial T}{\partial \theta}S_\theta \\ \dot{Q}_z = -\lambda\dfrac{\partial T}{\partial z}S_z \end{cases} \tag{B.5}$$

$$du = c_p dT \tag{B.6}$$

$$\rho c_p\frac{\partial T}{\partial t}dV = \frac{\partial}{\partial r}\left(\lambda\frac{\partial T}{\partial r}S_r\right)dr + \frac{\partial}{\partial \theta}\left(\lambda\frac{\partial T}{r\partial \theta}S_\theta\right)d\theta + \frac{\partial}{\partial z}\left(\lambda\frac{\partial T}{\partial z}S_z\right)dz + \dot{q}_v dV \tag{B.7}$$

Finally, by replacing the surfaces and the volume by its expressions, one obtains the differential equation for conduction heat transfer

Differential equation for conduction heat transfer

$$\rho c_p\frac{\partial T}{\partial t} = \frac{1}{r}\frac{\partial}{\partial r}\left(\lambda r\frac{\partial T}{\partial r}\right) + \frac{1}{r^2}\frac{\partial}{\partial \theta}\left(\lambda\frac{\partial T}{\partial \theta}\right) + \frac{\partial}{\partial z}\left(\lambda\frac{\partial T}{\partial z}\right) + \dot{q}_v \tag{B.8}$$

where λ stands for the thermal conductivity of the material and, c_p as the specific heat coefficient at constant pressure of the material.

Convection

In the following section, the main equations of convective heat transfer in integral and differential form will be presented [23].

Mass conservation

The mass conservation or continuity equation of an open system for a static control volume is the following

$$\frac{\partial}{\partial t}\int_{CV}\rho\, dV + \int_{CS}\rho\boldsymbol{v}\cdot\boldsymbol{n}\, dS = 0 \tag{B.9}$$

where CV stands for control volume, CS for control surface, ρ is the density of the fluid, $\boldsymbol{v}$ is the fluid velocity vector and $\boldsymbol{n}$ is the normal unit vector of the CS.

Mass conservation equation

$$\frac{\partial\rho}{\partial t} + \boldsymbol{\nabla}\cdot(\rho\boldsymbol{v}) = 0 \tag{B.10}$$

Analysis of the terms in equation (B.10) from left to right:

(i) Accumulated mass in the CV

(ii) Net flux of mass through the CV surfaces

Linear momentum conservation

The linear momentum conservation equation of an open system for a static control volume is the following

$$\frac{\partial}{\partial t}\int_{CV}\boldsymbol{v}\rho\, dV + \int_{CS}\boldsymbol{v}\rho\boldsymbol{v}\cdot\boldsymbol{n}\, dS = \int_{CS}\boldsymbol{f_n}\, dS + \int_{CV}\boldsymbol{f}_b\, dV \tag{B.11}$$

where $\boldsymbol{f_n}$ represents the superficial forces and $\boldsymbol{f}_b$ represents the body forces (per unit surface and volume, respectively).

Linear momentum conservation equation

$$\frac{\partial(\rho\boldsymbol{v})}{\partial t} + \boldsymbol{\nabla}\cdot(\rho\boldsymbol{v}\boldsymbol{v}) = -\boldsymbol{\nabla}p + \boldsymbol{\nabla}\cdot\boldsymbol{\tau} + \rho\boldsymbol{g} + \boldsymbol{f}^e \tag{B.12}$$

where p is the pressure applied to the control volume surfaces, $\boldsymbol{\tau}$ is the viscous stress tensor of the viscous forces applied to the control volume surfaces

$$\boldsymbol{\tau} = \begin{bmatrix} \tau_{rr} & \tau_{r\theta} & \tau_{rz} \\ \tau_{r\theta} & \tau_{\theta\theta} & \tau_{\theta z} \\ \tau_{rz} & \tau_{\theta z} & \tau_{zz} \end{bmatrix} = \mu(\boldsymbol{\nabla}\boldsymbol{v} + \boldsymbol{\nabla}\boldsymbol{v}^T) - \frac{2}{3}\mu(\boldsymbol{\nabla}\cdot\boldsymbol{v})\boldsymbol{\delta}$$

$\boldsymbol{g}$ is the gravitational acceleration vector and, $\boldsymbol{f}^e = \boldsymbol{j}\times\boldsymbol{B}$ is the electromagnetic force vector.

Analysis of the terms in equation (B.12) from left to right:

(i) Accumulated momentum in the CV

(ii) Net flux of momentum through the CV surfaces

(iii) Pressure forces on the CV surfaces

(iv) Viscous forces on the CV surfaces

(v) Gravitational force in the volume

(vi) Electromagnetic force in the volume

Energy conservation

The total energy conservation equation of an open system for a static control volume is the following

$$\frac{\partial}{\partial t}\int_{CV} e\rho\, dV + \int_{CS} e\rho \boldsymbol{v}\cdot\boldsymbol{n}\, dS = -\int_{CS} \dot{\boldsymbol{q}}^{(c+r)}\cdot\boldsymbol{n}\, dS + \int_{CS} \boldsymbol{v}\cdot\boldsymbol{f_n}\, dS + \int_{CV} \rho\boldsymbol{v}\cdot\boldsymbol{g}\, dV + \int_{CV} \boldsymbol{E}\cdot\boldsymbol{j}\, dV \tag{B.13}$$

where e is the total energy, $\dot{\boldsymbol{q}}^{(c+r)}$ is the heat flux of the combined effects of conduction and radiation and, the last term takes into account the heat losses of the Joule effect.

Total energy equation

$$\frac{\partial(\rho e)}{\partial t} + \boldsymbol{\nabla}\cdot(\rho\boldsymbol{v}e) = -\boldsymbol{\nabla}\cdot\boldsymbol{q}^{(c+r)} - \boldsymbol{\nabla}\cdot(p\boldsymbol{v}) + \boldsymbol{\nabla}\cdot(\boldsymbol{v}\cdot\boldsymbol{\tau}) + \rho\boldsymbol{v}\cdot\boldsymbol{g} + \boldsymbol{E}\cdot\boldsymbol{j} \tag{B.14}$$

Analysis of the terms in equation (B.14) from left to right:

(i) Accumulated energy in the CV

(ii) Net flux of energy through the CV surfaces

(iii) Convection and radiation heat flux (through molecular interaction and electromagnetic radiation, respectively).

(iv) Work of the pressure forces

(v) Work of the viscous forces

(vi) Work of the gravitational forces

(vii) Heat losses through the Joule effect

Since the total energy can be expressed as the sum of the internal and kinetic energy ($e = u + e_c$), one can derive also the kinetic and thermal energy conservation equations.

The kinetic energy conservation equation of an open system for a static control volume is the same as equation (B.12) but multiplied by the velocity vector.

$$\boldsymbol{v}\cdot[\text{eq. (B.12)}] \tag{B.15}$$

However, the kinetic energy can be expressed as $e_c = \boldsymbol{v}\cdot\boldsymbol{v}/2$

Kinetic energy equation

$$\frac{\partial(\rho e_c)}{\partial t} + \rho\boldsymbol{v}\cdot\boldsymbol{\nabla}e_c = -\boldsymbol{\nabla}\cdot(p\boldsymbol{v}) + p\boldsymbol{\nabla}\cdot\boldsymbol{v} + \boldsymbol{\nabla}\cdot(\boldsymbol{v}\cdot\boldsymbol{\tau}) - \boldsymbol{\tau}:\boldsymbol{\nabla}\boldsymbol{v} + \rho\boldsymbol{v}\cdot\boldsymbol{g} + \boldsymbol{v}\cdot\boldsymbol{f}^e \tag{B.16}$$

Analysis of the terms in equation (B.16) from left to right:

(i) Accumulated kinetic energy in the CV

(ii) Net flux of kinetic energy through the CV surfaces

(iii) Work of the pressure forces

(iv) Term related to the expansion/compression of the CV

(v) Work of the viscous forces

(vi) Viscous dissipation term. From Plank postulate ($\boldsymbol{\tau} : \boldsymbol{\nabla v} \geq 0$), this term will always dissipate energy, since it appears with a negative sign in the equation.

(vii) Work of the gravitational forces

(viii) Work of the electromagnetic forces

The thermal energy conservation equation of an open system for a static control volume is derived when (B.16) is introduced in equation (B.14).

Thermal energy equation

$$\frac{\partial(\rho u)}{\partial t} + \rho\, \boldsymbol{v} \cdot \boldsymbol{\nabla} u = -\boldsymbol{\nabla} \cdot \boldsymbol{q}^{(c+r)} - p \boldsymbol{\nabla} \cdot \boldsymbol{v} + \boldsymbol{\tau} : \boldsymbol{\nabla v} + \Phi^e \tag{B.17}$$

where u is the internal energy of the CV and, Φ^e is the heat loss due to the Joule effect

$$\Phi^e = \boldsymbol{E} \cdot \boldsymbol{j} = \boldsymbol{j} \cdot \boldsymbol{j} / \sigma_e$$

Analysis of the terms in equation (B.17) from left to right:

(i) Accumulated internal energy in the CV

(ii) Net flux of internal energy through the CV surfaces

(iii) Convection and radiation heat flux (through molecular interaction and electromagnetic radiation, respectively).

(iv) Term related to the expansion/compression of the CV

(v) Viscous dissipation term. In this case appears with a positive sign, since this term will always increase the internal energy.

(vi) Heat losses through the Joule effect

Appendix C

Transport properties computation

The thermal transport properties such as specific heat at constant pressure C_p, thermal conductivity λ and viscosity η are needed to develop the heat transfer calculations, since the properties of the working fluid must be known. This appendix presents the methodology employed to compute such properties based on tabulated data and analytic expressions.

Reference [24] presents three expressions to compute the thermal transport properties of the mixture, based on the properties of each individual species, their molecular weights, and their respective molar fractions.

$$C_{p,\text{mix}} = \frac{\sum_{i=1}^{\text{NM}} x_i C^{\circ}_{p,i}}{\sum_{i=1}^{\text{NM}} x_i M_i} \tag{C.1}$$

$$\eta_{\text{mix}} = \sum_{i=1}^{NM} \frac{x_i \eta_i}{x_i + \sum_{j=1}^{NM} x_j \phi_{ij}} \tag{C.2}$$

$$\lambda_{\text{mix}} = \sum_{i=1}^{\text{NM}} \frac{x_i \lambda_i}{x_i + \sum_{j=1}^{\text{NM}} x_j \Psi_{ij}} \tag{C.3}$$

where

$$\phi_{ij} = \frac{1}{4}\left[1 + \left(\frac{\eta_i}{\eta_j}\right)^{1/2}\left(\frac{M_j}{M_i}\right)^{1/4}\right]^2 \left(\frac{2M_j}{M_i + M_j}\right)^{1/2} \tag{C.4}$$

and

$$\Psi_{ij} = \phi_{ij}\left[1 + \frac{2.41\,(M_i - M_j)\,(M_i - 0.142 M_j)}{(M_i + M_j)^2}\right] \tag{C.5}$$

The individual properties of the species have been computed through the tabulated coefficients publishe by NASA in [25], where the properties are computed as

$$\frac{C_p^o(T)}{R} = a_1 + a_2 T + a_3 T^2 + a_4 T^3 + a_5 T^4 \tag{C.6}$$

$$\left.\begin{matrix}\ln(\eta) \\ \ln(\lambda)\end{matrix}\right\} = A \ln(T) + \frac{B}{T} + \frac{C}{T^2} + D \tag{C.7}$$

Figures C.1 and C.2 show as an example, the coefficients used to compute the c_p, λ and η of the CO_2 present in a mixture.

```
COS               J 3/61C  1.0  1.S  1.   0.G   300.000  5000.000     60.07640 1   Chase (1985)
 5.23920000E+00 2.41005840E-03-9.60645220E-07 1.77783470E-10-1.22357040E-14    2
-1.84804550E+04-3.07773889E+00 2.46253210E+00 1.19479920E-02-1.37943700E-05    3
 8.07077360E-09-1.83276530E-12-1.78039870E+04 1.08058688E+01-1.66455205E+04    4
CO2               L 7/88C  1.0  2.   0.   0.G   200.000  6000.000     44.00980 1   Gurvich (1991)
 4.63659493E+00 2.74131991E-03-9.95828531E-07 1.60373011E-10-9.16103468E-15    2
-4.90249341E+04-1.93534855E+00 2.35677352E+00 8.98459677E-03-7.12356269E-06    3
 2.45919022E-09-1.43699548E-13-4.83719697E+04 9.90105222E+00-4.73281047E+04    4
CO2+              L10/92C  1.0  2.E -1.   0.G   298.150  6000.000     44.00925 1   Gurvich (1991)
 5.61292513E+00 1.89829994E-03-7.34596383E-07 1.23975665E-10-7.57692288E-15    2
 1.11621136E+05-5.65135703E+00 3.39305653E+00 5.82300415E-03 4.38012075E-08    3
-4.68236271E-09 2.31552825E-12 1.12356151E+05 6.39038548E+00 1.13618832E+05    4
COOH              TPIS91C  1.0  2.H  1.   0.G   200.000  6000.000     45.01774 1   Gurvich (1991)
 5.39206247E+00 4.11221305E-03-1.48194817E-06 2.39875278E-10-1.43902965E-14    2
-2.76708786E+04-2.23528631E+00 2.92207915E+00 7.62453820E-03 3.29884683E-06    3
-1.07135249E-08 5.11587309E-12-2.68383588E+04 1.12925989E+01-2.56178656E+04    4
```

Figure C.1: Specific heat coefficients of CO_2 highlighted in blue. Source: [25].

```
COS                                 V2C2  GORDON; NASA TM86885, OCT 1984
 V  300.000 1000.000 0.52969284E 00-0.26892616E 03 0.17742103E 05 0.25013200E 01
 V 1000.000 5000.000 0.63342607E 00-0.33447711E 02-0.54409462E 05 0.16208681E 01
 C  300.000 1000.000 0.57101414E 00-0.41050507E 03 0.26688182E 05 0.26183777E 01
 C 1000.000 5000.000 0.67257356E 00-0.89956888E 02-0.91877099E 05 0.17124897E 01
CO2                                 V2C2  GORDON; NASA TM86885, OCT 1984
 V  300.000 1000.000 0.54330318E 00-0.18823898E 03 0.88726567E 04 0.24499362E 01
 V 1000.000 5000.000 0.65318879E 00 0.51738759E 02-0.62834882E 05 0.15227045E 01
 C  300.000 1000.000 0.53726173E 00-0.49928331E 03 0.37397504E 05 0.32903619E 01
 C 1000.000 5000.000 0.66068182E 00-0.12741845E 03-0.81580328E 05 0.21817907E 01
CP                                  V2C2  GORDON; NASA TM86885, OCT 1984
 V  300.000 1000.000 0.55142210E 00-0.16522371E 03 0.67076536E 04 0.20562199E 01
 V 1000.000 5000.000 0.65372263E 00 0.51025907E 02-0.55485385E 05 0.11956174E 01
 C  300.000 1000.000 0.59035579E 00-0.26133699E 03 0.16965587E 05 0.20433882E 01
 C 1000.000 5000.000 0.67681979E 00 0.43561992E 02-0.90694254E 05 0.12456589E 01
CS                                  V2C2  GORDON; NASA TM86885, OCT 1984
 V  300.000 1000.000 0.56203230E 00-0.13600215E 03 0.42677153E 04 0.20800917E 01
 V 1000.000 5000.000 0.65429610E 00 0.47958932E 02-0.44621677E 05 0.13080095E 01
 C  300.000 1000.000 0.61122836E 00-0.22957023E 03 0.15067012E 05 0.19653352E 01
 C 1000.000 5000.000 0.86597093E 00 0.73832733E 03-0.37667638E 06-0.37818229E 00
```

Figure C.2: Viscosity and thermal conductivity coefficients of CO_2 highlighted in yellow and green, respectively. Source: [25].

Appendix D

Lineal elastostatic equations in cylindrical coordinates

The governing equations of lineal elastostatics are presented in this appendix for an axisymmetric body in the cylindrical coordinate form.

Definitions

As a reminder, the cylindrical reference system defines the position in space of an arbitrary point P by the following three real numbers: (r, θ, z). Where r denotes the radial distance from a chosen reference axis, θ denotes the azimuth angle with respect to a chosen reference direction and z denotes the height from a chosen reference plane (perpendicular to the reference axis). This can be easily seen in figure D.1 (note that the radial distance r is presented with the letter ρ).

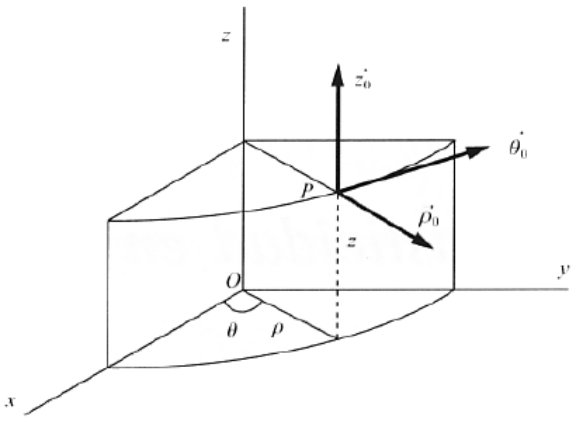

Figure D.1: Cylindrical coordinate reference system (Source: [26]).

By applying this reference system to the elemental vicinity of a point P, one can define the elemental parallelepiped of length dr, $rd\theta$ and dz (see figure D.2) and, define the corresponding stress and strain tensors acting on it.

$$\boldsymbol{\sigma} = \begin{bmatrix} \sigma_{rr} & \tau_{r\theta} & \tau_{rz} \\ \tau_{r\theta} & \sigma_{\theta\theta} & \tau_{\theta z} \\ \tau_{rz} & \tau_{\theta z} & \sigma_{zz} \end{bmatrix} \tag{D.1}$$

$$\boldsymbol{\varepsilon} = \begin{bmatrix} \varepsilon_{rr} & \varepsilon_{r\theta} & \varepsilon_{rz} \\ \varepsilon_{r\theta} & \varepsilon_{\theta\theta} & \varepsilon_{\theta z} \\ \varepsilon_{rz} & \varepsilon_{\theta z} & \varepsilon_{zz} \end{bmatrix} = \begin{bmatrix} \varepsilon_{rr} & \frac{1}{2}\gamma_{r\theta} & \frac{1}{2}\gamma_{rz} \\ \frac{1}{2}\gamma_{r\theta} & \varepsilon_{\theta\theta} & \frac{1}{2}\gamma_{\theta z} \\ \frac{1}{2}\gamma_{rz} & \frac{1}{2}\gamma_{\theta z} & \varepsilon_{zz} \end{bmatrix} \tag{D.2}$$

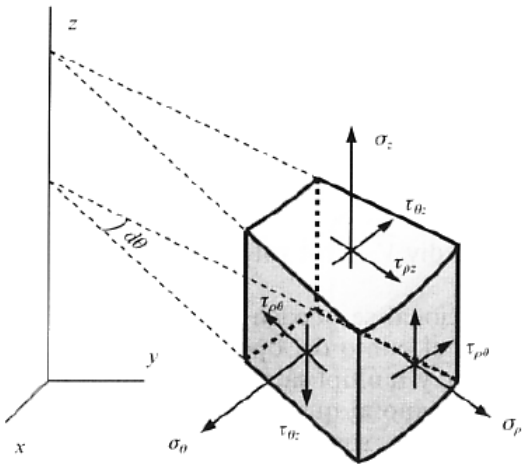

Figure D.2: Cylindrical stresses acting on the faces of the infinitesimal parallelepiped in the elemental vicinity of a point P (Source: [26]).

However, for an axisymmetric body with axisymmetrical boundary conditions, the stresses and strains become independent of the θ coordinate, thus, simplifying the problem from three dimensions to only two (see figure D.3).

The stress and strain tensors would then become

$$\boldsymbol{\sigma} = \begin{bmatrix} \sigma_{rr} & 0 & \tau_{rz} \\ 0 & \sigma_{\theta\theta} & 0 \\ \tau_{rz} & 0 & \sigma_{zz} \end{bmatrix} \tag{D.3}$$

$$\boldsymbol{\varepsilon} = \begin{bmatrix} \varepsilon_{rr} & 0 & \varepsilon_{rz} \\ 0 & \varepsilon_{\theta\theta} & 0 \\ \varepsilon_{rz} & 0 & \varepsilon_{zz} \end{bmatrix} = \begin{bmatrix} \varepsilon_{rr} & 0 & \frac{1}{2}\gamma_{rz} \\ 0 & \varepsilon_{\theta\theta} & 0 \\ \frac{1}{2}\gamma_{rz} & 0 & \varepsilon_{zz} \end{bmatrix} \tag{D.4}$$

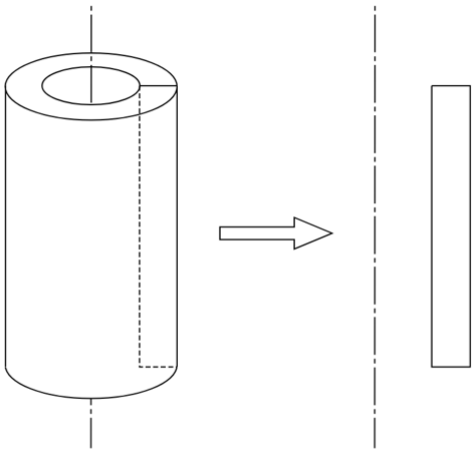

Figure D.3: Simplification from a 3D to a 2D analysis of an axisymmetric body by analyzing the cross-section only. Note that an axisymmetric body can be seen as a structure of revolution, generated by rotating the cross-section around a revolution axis.

In the vast majority of the literature, the principal terms of the above tensors receive specific names such as:

- σ_{rr}: radial stress
- $\sigma_{\theta\theta}$: hoop/circumferential/azimuthal stress
- σ_{zz}: axial/longitudinal stress
- ε_{rr}: radial strain
- $\varepsilon_{\theta\theta}$: hoop/circumferential/azimuthal strain
- ε_{zz}: axial/longitudinal strain

The displacement field can also be expressed with cylindrical coordinates in the form of

$$\boldsymbol{u} = \begin{bmatrix} u_r \\ u_z \end{bmatrix} \tag{D.5}$$

Strain-displacement Relations

The strain-displacement relations, or also called compatibility equations, relate the strain tensor ($\boldsymbol{\varepsilon}$) with the displacement field ($\boldsymbol{u}$) in the form of 4 partial differential equations (with 6 unknowns) [27].

Compatibility equations

$$\begin{aligned} \varepsilon_{rr} &= \frac{\partial u_r}{\partial r} & \varepsilon_{zz} &= \frac{\partial u_z}{\partial z} \\ \varepsilon_{\theta\theta} &= \frac{1}{r}\left(\frac{\partial u_\theta}{\partial \theta} + u_r\right) & \varepsilon_{rz} &= \frac{1}{2}\gamma_{rz} = \frac{1}{2}\left(\frac{\partial u_r}{\partial z} + \frac{\partial u_z}{\partial r}\right) \end{aligned} \tag{D.6}$$

Generalized Hooke's Law

The generalized Hooke's law, or the also called constitutive equations, relates the strain ($\boldsymbol{\varepsilon}$) and the stress ($\boldsymbol{\sigma}$) tensor through 4 simple equations [26][28][29]. Those are the same in cylindrical and Cartesian coordinates, the only thing that changes is the nomenclature.

Constitutive equations

$$\begin{aligned} \varepsilon_{rr} &= \frac{1}{E}\left[\sigma_{rr} - \nu\left(\sigma_{\theta\theta} + \sigma_z\right)\right] & \varepsilon_{zz} &= \frac{1}{E}\left[\sigma_{zz} - \nu\left(\sigma_{rr} + \sigma_{\theta\theta}\right)\right] \\ \varepsilon_{\theta\theta} &= \frac{1}{E}\left[\sigma_{\theta\theta} - \nu\left(\sigma_{rr} + \sigma_{zz}\right)\right] & \gamma_{rz} &= \frac{\tau_{rz}}{G} \end{aligned} \tag{D.7}$$

where E is the longitudinal elastic modulus (also Young modulus) and ν is the Poisson coefficient of the material.

However, equations (D.7) are only valid for isotropic materials.

Equations (D.7) can also be expressed in a more compact form such as equations (D.8) or (D.10). In the first case, the $\boldsymbol{C^{-1}}$ term is called the compliance matrix, while the $\boldsymbol{C}$ term is called the elasticity matrix.

$$\boldsymbol{\varepsilon} = \boldsymbol{C^{-1}\sigma} \tag{D.8}$$

$$\boldsymbol{C^{-1}} = \begin{bmatrix} \frac{1}{E} & -\frac{\nu}{E} & -\frac{\nu}{E} & 0 \\ -\frac{\nu}{E} & \frac{1}{E} & -\frac{\nu}{E} & 0 \\ -\frac{\nu}{E} & -\frac{\nu}{E} & \frac{1}{E} & 0 \\ 0 & 0 & 0 & \frac{1}{G} \end{bmatrix} \tag{D.9}$$

$$\boldsymbol{\sigma} = \boldsymbol{C\varepsilon} \tag{D.10}$$

$$\boldsymbol{C} = \begin{bmatrix} \lambda + 2\mu & \lambda & \lambda & 0 \\ \lambda & \lambda + 2\mu & \lambda & 0 \\ \lambda & \lambda & \lambda + 2\mu & 0 \\ 0 & 0 & 0 & \mu \end{bmatrix} \tag{D.11}$$

Those equations can also be expressed with the Lamé parameters λ and μ, which relate to E and ν through equations (D.12)

$$\lambda = \frac{\nu E}{(1+\nu)(1-2\nu)} \qquad \mu = G = \frac{E}{2(1+\nu)} \tag{D.12}$$

where G is the transverse elastic modulus (also shear modulus).

Equilibrium

The 2 partial differential equations of equilibrium of linear elastostatics in cylindrical coordinates (with 4 unknowns) are presented below [26][27]

Equilibrium equations

$$\begin{aligned} \frac{\partial \sigma_{rr}}{\partial r} + \frac{\sigma_{rr} - \sigma_{\theta\theta}}{r} + \frac{\partial \tau_{rz}}{\partial z} + f_r = 0 \\ \frac{\partial \sigma_{zz}}{\partial z} + \frac{\partial \tau_{rz}}{\partial r} + \frac{\tau_{rz}}{r} + f_z = 0 \end{aligned} \tag{D.13}$$

where (f_r, f_z) are body force components per unit volume.

Boundary Conditions

There are two types of boundary conditions applied on the boundary Γ.

The first ones are the Dirichlet boundary conditions, in which the displacements $\bar{u}^i$ are prescribed on boundaries Γ_u^i $(i = r, z)$ [29].

$$\begin{cases} u_r = \bar{u}^r & \text{on } \Gamma_u^r \\ u_z = \bar{u}^z & \text{on } \Gamma_u^z \end{cases} \tag{D.14}$$

The second ones are the Neumann boundary conditions, in which the tractions $\bar{t}^i$ are prescribed on boundaries Γ_σ^i $(i = r, z)$ [27][29].

$$\begin{cases} \sigma_r \hat{n}_r + \tau_{r\theta} \hat{n}_\theta + \tau_{rz} \hat{n}_z = \bar{t}^r & \text{on } \Gamma_\sigma^r \\ \tau_{rz} \hat{n}_r + \tau_{\theta z} \hat{n}_\theta + \sigma_z \hat{n}_z = \bar{t}^z & \text{on } \Gamma_\sigma^z \end{cases} \tag{D.15}$$

Boundary Value Problem

There are two ways to formulate the boundary value problem, one of them is through the Strong Form and the other one is through the Weak Form.
The former is the easiest one to derive and groups all the equations seen at the moment in this appendix. The latter is employed in Finite Element Method (FEM) softwares, as it is easier to solve numerically since it implies first-order derivatives (unlike the strong form, which has second derivatives of the displacement).

In order to define the domain of the problem, let $\Omega \subset \mathbb{R}^3$ be an open set with piecewise smooth boundary Γ, where the union of the set with its boundary is $\bar{\Omega} = \Omega \cup \Gamma$.
The boundary Γ admits the decomposition

$$\Gamma = \Gamma_u^i \cup \Gamma_\sigma^i$$

where

$$\Gamma_u^i \cap \Gamma_\sigma^i = \varnothing$$

The formulation of the problem can be stated as follows:

Strong formulation

Given $f_i\colon \Omega \to \mathbb{R}$, $\bar{u}^i\colon \Gamma_u^i \to \mathbb{R}$, $\bar{t}^i\colon \Gamma_\sigma^i \to \mathbb{R}$, find $u_i\colon \bar{\Omega} \to \mathbb{R}$ such that

$$\begin{cases} \dfrac{\partial \sigma_{rr}}{\partial r} + \dfrac{\sigma_{rr} - \sigma_{\theta\theta}}{r} + \dfrac{\partial \tau_{rz}}{\partial z} + f_r = 0 \\ \dfrac{\partial \sigma_{zz}}{\partial z} + \dfrac{\partial \tau_{rz}}{\partial r} + \dfrac{\tau_{rz}}{r} + f_z = 0 \end{cases} \quad \text{in } \Omega \tag{D.16}$$

$$u_i = \bar{u}^i \qquad \text{on } \Gamma_u^i \tag{D.17}$$

$$\sigma_{ij} n_j = \bar{t}^i \qquad \text{on } \Gamma_\sigma^i \tag{D.18}$$

where $\boldsymbol{\sigma}$ follows constitutive equations (D.10) and $\boldsymbol{\varepsilon}$ follows compatibility equations (D.6).

To understand the weak formulation, one must first introduce the following concepts [30][31]:

- **Test functions**

$$\mathcal{V} = \left\{ v_i : \bar{\Omega} \to \mathbb{R} \middle| \text{ continuous with square-integrable derivative, } v_i = 0 \text{ on } \Gamma_u^i \right\}$$

- **Trial functions**

$$\mathcal{S} = \left\{ u_i : \bar{\Omega} \to \mathbb{R} \middle| \text{ continuous with square-integrable derivative, } u_i = \bar{u}^i \text{ on } \Gamma_u^i \right\}$$

where $i = r, z$.

- **Voigt notation**

This notation simplifies the writing of symmetric second-order tensors by writing them as column vectors through a process called Voigt rule. This rule depends on whether the tensor represents a kinetic or kinematic quantity:

– Kinetic Voigt Rule

$$\boldsymbol{\sigma} = \begin{bmatrix} \sigma_{rr} & 0 & \tau_{rz} \\ 0 & \sigma_{\theta\theta} & 0 \\ \tau_{rz} & 0 & \sigma_{zz} \end{bmatrix} = \begin{bmatrix} \sigma_{rr} \\ \sigma_{\theta\theta} \\ \sigma_{zz} \\ \tau_{rz} \end{bmatrix} \tag{D.19}$$

– Kinematic Voigt Rule

$$\boldsymbol{\varepsilon} = \begin{bmatrix} \varepsilon_{rr} & 0 & \varepsilon_{rz} \\ 0 & \varepsilon_{\theta\theta} & 0 \\ \varepsilon_{rz} & 0 & \varepsilon_{zz} \end{bmatrix} = \begin{bmatrix} \varepsilon_{rr} & 0 & \frac{1}{2}\gamma_{rz} \\ 0 & \varepsilon_{\theta\theta} & 0 \\ \frac{1}{2}\gamma_{rz} & 0 & \varepsilon_{zz} \end{bmatrix} = \begin{bmatrix} \varepsilon_{rr} \\ \varepsilon_{\theta\theta} \\ \varepsilon_{zz} \\ \gamma_{rz} \end{bmatrix} \tag{D.20}$$

Note that the shear strains are multiplied by 2.

Now, the equilibrium equations, which are the starting point of the process, will be rewritten in vectorial notation for the ease of the procedure.

$$\begin{cases} \dfrac{\partial \sigma_{rr}}{\partial r} + \dfrac{\sigma_{rr} - \sigma_{\theta\theta}}{r} + \dfrac{\partial \tau_{rz}}{\partial z} + f_r = 0 \\ \dfrac{\partial \sigma_{zz}}{\partial z} + \dfrac{\partial \tau_{rz}}{\partial r} + \dfrac{\tau_{rz}}{r} + f_z = 0 \end{cases} \implies \begin{cases} \boldsymbol{\nabla} \cdot \boldsymbol{\sigma}_r - \dfrac{\sigma_{\theta\theta}}{r} + f_r = 0 \\ \boldsymbol{\nabla} \cdot \boldsymbol{\sigma}_z + f_z = 0 \end{cases} \tag{D.21}$$

where $\boldsymbol{\sigma}_r = \begin{bmatrix} \sigma_{rr} \\ 0 \\ \tau_{rz} \end{bmatrix}$ and $\boldsymbol{\sigma}_r = \begin{bmatrix} \tau_{rz} \\ 0 \\ \sigma_{zz} \end{bmatrix}$.

To obtain the Weak Form, the equilibrium equations must be multiplied by the test function and integrated over the domain as follows

$$\begin{cases} \displaystyle\int_\Omega v_r (\boldsymbol{\nabla} \cdot \boldsymbol{\sigma}_r - \frac{\sigma_{\theta\theta}}{r} + f_r)\, d\Omega = 0 \\ \displaystyle\int_\Omega v_z (\boldsymbol{\nabla} \cdot \boldsymbol{\sigma}_z + f_z)\, d\Omega = 0 \end{cases} \tag{D.22}$$

Rearranging the terms

$$\begin{cases} \displaystyle\int_\Omega v_r (\boldsymbol{\nabla} \cdot \boldsymbol{\sigma}_r)\, d\Omega - \int_\Omega v_r \frac{\sigma_{\theta\theta}}{r}\, d\Omega + \int_\Omega v_r f_r\, d\Omega = 0 \\ \displaystyle\int_\Omega v_z (\boldsymbol{\nabla} \cdot \boldsymbol{\sigma}_z)\, d\Omega + \int_\Omega v_z f_z\, d\Omega = 0 \end{cases} \tag{D.23}$$

and applying Green's theorem to the first terms of the above equations, yields

$$\begin{cases} \displaystyle\int_\Gamma v_r (\boldsymbol{\sigma}_r \cdot \boldsymbol{n})\, d\Gamma - \int_\Omega \boldsymbol{\nabla} v_r \cdot \boldsymbol{\sigma}_r \; d\Omega - \int_\Omega v_r \frac{\sigma_{\theta\theta}}{r}\, d\Omega + \int_\Omega v_r f_r\, d\Omega = 0 \\ \displaystyle\int_\Gamma v_z (\boldsymbol{\sigma}_z \cdot \boldsymbol{n})\, d\Gamma - \int_\Omega \boldsymbol{\nabla} v_z \cdot \boldsymbol{\sigma}_z \; d\Omega + \int_\Omega v_z f_z\, d\Omega = 0 \end{cases} \tag{D.24}$$

Combining the two equations and recalling the definition of the test function that states that $\boldsymbol{v}$ vanishes on Γ_u^i, the following is obtained

$$\int_\Omega (\boldsymbol{\nabla} v_r \cdot \boldsymbol{\sigma}_r + \boldsymbol{\nabla} v_z \cdot \boldsymbol{\sigma}_z)\, d\Omega = \int_{\Gamma_\sigma} \left[v_r (\boldsymbol{\sigma}_r \cdot \boldsymbol{n}) + v_z (\boldsymbol{\sigma}_z \cdot \boldsymbol{n}) \right] d\Gamma + \int_\Omega (v_r f_r + v_z f_z)\, d\Omega - \int_\Omega v_r \frac{\sigma_{\theta\theta}}{r}\, d\Omega \tag{D.25}$$

Applying the Neumann boundary condition, this can be rewritten as

$$\int_\Omega (\boldsymbol{\nabla} v_r \cdot \boldsymbol{\sigma}_r + \boldsymbol{\nabla} v_z \cdot \boldsymbol{\sigma}_z)\, d\Omega = \int_{\Gamma_\sigma} \boldsymbol{v} \cdot \bar{\boldsymbol{t}}\, d\Gamma + \int_\Omega \boldsymbol{v} \cdot \boldsymbol{f}\, d\Omega - \int_\Omega v_r \frac{\sigma_{\theta\theta}}{r}\, d\Omega \tag{D.26}$$

where, rearranging the terms gives

$$\int_\Omega (\boldsymbol{\nabla} v_r \cdot \boldsymbol{\sigma}_r + \boldsymbol{\nabla} v_z \cdot \boldsymbol{\sigma}_z + v_r \frac{\sigma_{\theta\theta}}{r})\, d\Omega = \int_{\Gamma_\sigma} \boldsymbol{v} \cdot \bar{\boldsymbol{t}}\, d\Gamma + \int_\Omega \boldsymbol{v} \cdot \boldsymbol{f}\, d\Omega \tag{D.27}$$

At this point, the symmetric gradient operator using Voigt notation will be introduced, through a new definition of the strain tensor.

Symmetric gradient operator in Voigt notation ($\boldsymbol{\nabla}^s$)

$$\boldsymbol{\varepsilon} = \begin{bmatrix} \varepsilon_r \\ \varepsilon_\theta \\ \varepsilon_z \\ \gamma_{rz} \end{bmatrix} = \begin{bmatrix} \frac{\partial u_r}{\partial r} \\ \frac{u_r}{r} \\ \frac{\partial u_z}{\partial z} \\ \frac{\partial u_r}{\partial z} + \frac{\partial u_z}{\partial r} \end{bmatrix} = \boldsymbol{\nabla}^s \boldsymbol{u} \tag{D.28}$$

$$\boldsymbol{\nabla}^s := \begin{bmatrix} \frac{\partial}{\partial r} & 0 \\ \frac{1}{r} & 0 \\ 0 & \frac{\partial}{\partial z} \\ \frac{\partial}{\partial z} & \frac{\partial}{\partial r} \end{bmatrix} \tag{D.29}$$

Then, by taking into account the operator that has just been introduced, the first term of equation (D.27) can be rewritten as follows (note that it refers to the term inside the integral)

$$\boldsymbol{\nabla} v_r \cdot \boldsymbol{\sigma}_r + \boldsymbol{\nabla} v_z \cdot \boldsymbol{\sigma}_z + v_r \frac{\sigma_{\theta\theta}}{r} =$$

$$= \begin{bmatrix} (\frac{\partial v_r}{\partial r}) & (\frac{v_r}{r}) & (\frac{\partial v_z}{\partial z}) & (\frac{\partial v_z}{\partial r} + \frac{\partial v_r}{\partial z}) \end{bmatrix} \begin{bmatrix} \sigma_{rr} \\ \sigma_{\theta\theta} \\ \sigma_{zz} \\ \tau_{rz} \end{bmatrix} = (\boldsymbol{\nabla}^s \boldsymbol{v})^T \boldsymbol{\sigma} \tag{D.30}$$

Therefore, equation (D.27) becomes

$$\int_\Omega (\boldsymbol{\nabla}^s \boldsymbol{v})^T \boldsymbol{\sigma}\, d\Omega = \int_{\Gamma_\sigma} \boldsymbol{v} \cdot \bar{\boldsymbol{t}}\, d\Gamma + \int_\Omega \boldsymbol{v} \cdot \boldsymbol{f}\, d\Omega \tag{D.31}$$

and, by taking into account the constitutive equation,

$$\boldsymbol{\sigma} = \boldsymbol{C}\boldsymbol{\varepsilon} = \boldsymbol{C}\boldsymbol{\nabla}^s \boldsymbol{u} \tag{D.32}$$

the weak formulation of the problem states as follows

Weak formulation

Given $\boldsymbol{f}$: $\Omega \to \mathbb{R}^3$, $\bar{\boldsymbol{t}}$: $\Gamma_\sigma \to \mathbb{R}^3$, find $\boldsymbol{u} \in \mathcal{S}$ such that

$$\int_\Omega (\boldsymbol{\nabla}^s \boldsymbol{v})^T \boldsymbol{C} \boldsymbol{\nabla}^s \boldsymbol{u}\, d\Omega = \int_\Omega \boldsymbol{v}^T \boldsymbol{f}\, d\Omega + \int_{\Gamma_\sigma} \boldsymbol{v}^T \bar{\boldsymbol{t}}\, d\Gamma \qquad \forall \boldsymbol{v} \in \mathcal{V} \tag{D.33}$$

Appendix E

ProPEP 3 combustion results

All the information obtained from the propellant evaluation program is presented in this chapter of the appendix to support the results obtained throughout the thesis.

Figures E.1 and E.2 show snapshots of the program interface where the input data is introduced.

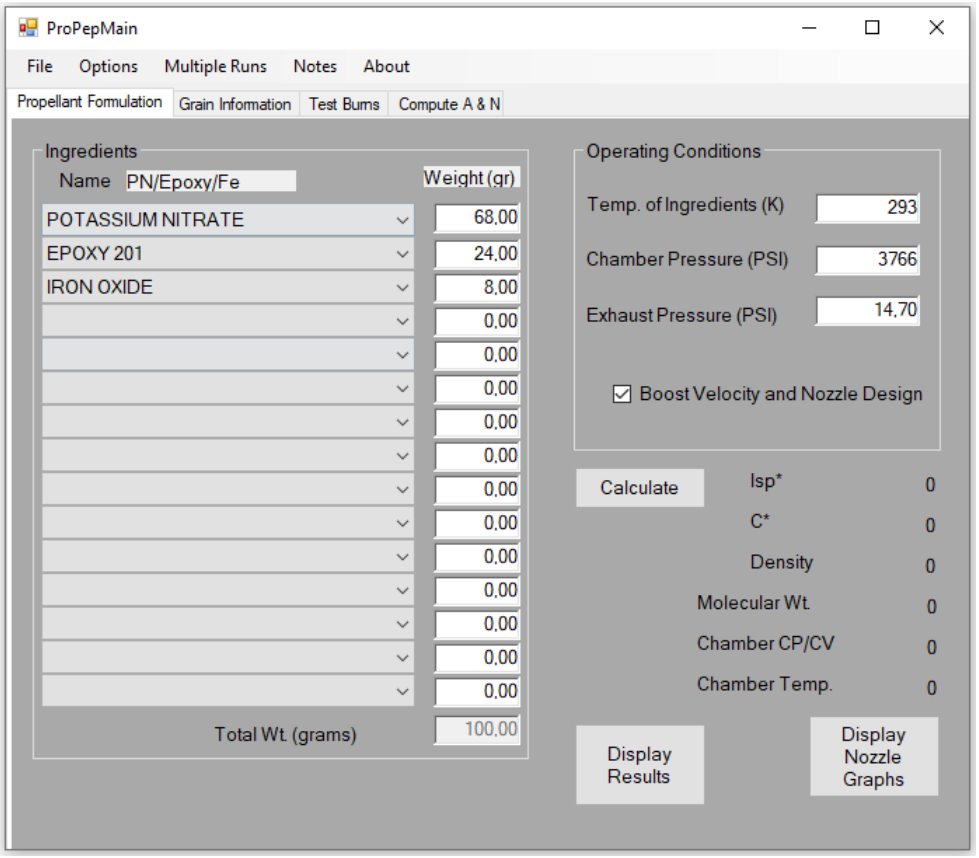

Figure E.1: PN/Epoxy/Fe propellant input data in ProPEP software.

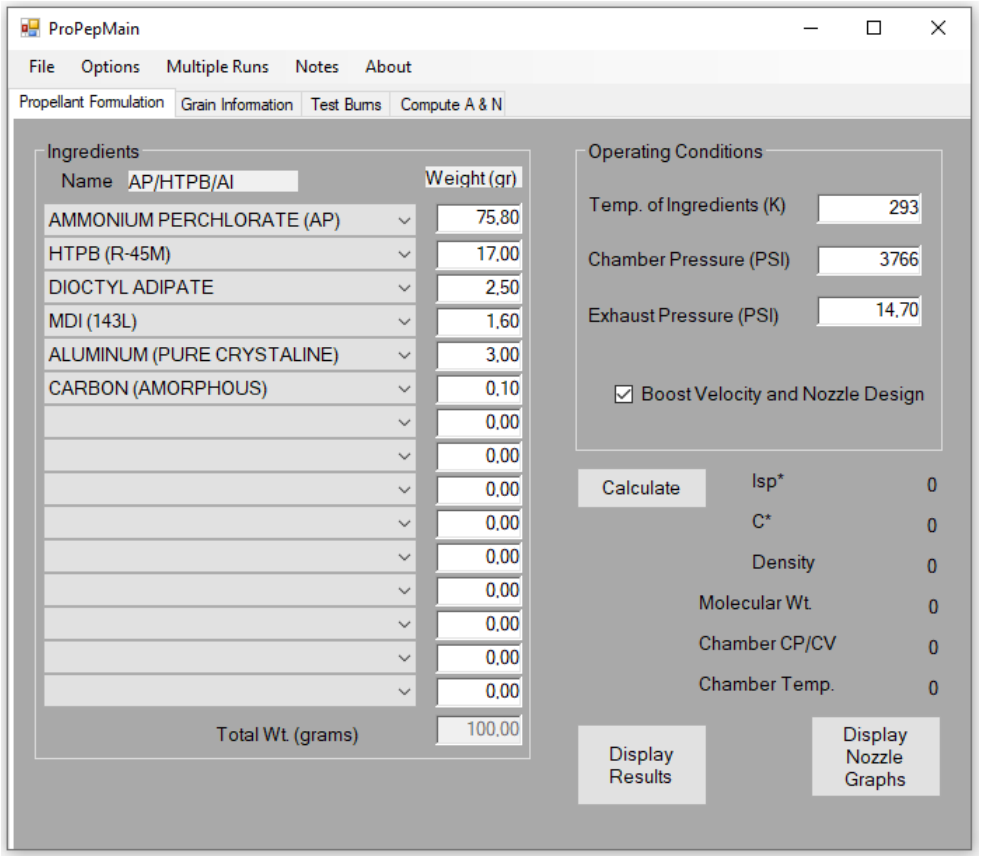

Figure E.2: AP/HTPB/Al propellant input data in ProPEP software.

The program outputs are presented in figures E.3 (for the PN/Epoxy/Fe propellant) and E.4 (for the AP/HTPB/Al propellant).

```
NUMBER OF GRAM ATOMS OF EACH ELEMENT PRESENT IN INGREDIENTS

    2,054443 H
    1,369629 C
    0,672548 N
    2,510334 O
    0,672548 K
    0,100188 FE

*****************************CHAMBER RESULTS FOLLOW    ******************************
  T(K)   T(F)   P(ATM)    P(PSI) ENTHALPY  ENTROPY    CP/CV     GAS    RT/V
  1528   2292    256,18   3766,00  -105,21    149,32  1,1346   2,340  109,433

SPECIFIC HEAT (MOLAR) OF GAS AND TOTAL =      9,137     14,122
NUMBER MOLS GAS AND CONDENSED =      2,340     0,436

 8,543465e-001 CO          6,546468e-001 H2          3,356177e-001 K2CO3*      3,351484e-001 N2
 3,135667e-001 H2O         1,515967e-001 CO2         6,907846e-002 Fe&         3,108529e-002 FeO&
 2,767599e-002 CH4         1,934918e-003 NH3         1,122107e-003 KHO         1,641160e-004 CNH
 9,875317e-005 KCN         6,046928e-005 K           4,958192e-005 CH2O        9,767385e-006 C2H4
 7,441903e-006 CNHO        7,197479e-006 FeH2O2      5,091463e-006 K2H2O2      1,960732e-006 CH3
  1,90236E-06 H            1,90236E-06 H

THE MOLECULAR WEIGHT OF THE MIXTURE IS     36,019
```

Figure E.3: Output file of the ProPEP software for the PN/Epoxy/Fe propellant.

```
NUMBER OF GRAM ATOMS OF EACH ELEMENT PRESENT IN INGREDIENTS

    4,806319 H
    1,496251 C
    0,656936 N
    2,631705 O
    0,111194 AL
    0,645123 CL

**************************CHAMBER RESULTS FOLLOW   ****************************
  T(K)  T(F)  P(ATM)   P(PSI) ENTHALPY  ENTROPY   CP/CV    GAS   RT/V
  2262  3612   256,18  3766,00   -54,29   234,22  1,2504  4,550   56,303

SPECIFIC HEAT (MOLAR) OF GAS AND TOTAL =     9,518     9,803
NUMBER MOLS GAS AND CONDENSED =     4,550    0,055

 1,338335e+000 CO         1,267546e+000 H2         8,118431e-001 H2O        6,435399e-001 HCl
 3,280473e-001 N2         1,575227e-001 CO2        5,539060e-002 Al2O3&     1,188552e-003 H
 6,482129e-004 NH3        4,346184e-004 Cl         3,307014e-004 AlCl3      1,293236e-004 CNH
 1,186714e-004 HO         1,002666e-004 CH4        5,909691e-005 CH2O       3,745782e-005 AlCl2
 1,827388e-005 CHO        1,099880e-005 CNHO       9,389879e-006 COCl       5,171528e-006 AlCl
 3,966990e-006 AlOCl      3,328898e-006 Cl2        3,053997e-006 NO         2,283608e-006 CH3
  1,90636E-06 NH2

THE MOLECULAR WEIGHT OF THE MIXTURE IS    21,714
```

Figure E.4: Output file of the ProPEP software for the AP/HTPB/Al propellant.

Appendix F

ANSYS Validation

The major concern when extracting results from numerical simulation software, like ANSYS, is to validate the results obtained and ensure they are solid and make total sense.
Therefore, the main objective of this chapter is to validate the numerical results presented in the report of this thesis by analyzing three problems of interest with an analytical solution.

The problems have been selected by taking into account several reasons such as simplicity, the existence of analytic solutions, similarity in terms of geometry and reference system concerning the solid rocket motor case, and resemblance in the theory involved.
The first case is an elastostatic problem, in which a long hollow cylinder is exposed to internal and external pressure. The second case is a thermal problem, which consists of the same cylinder but is now exposed to forced convection in the interior surface and natural convection in the exterior surface. Finally, the third case is a thermoelastic problem. In this last case, the cylinder is exposed to the pressure and thermal loads of cases one and two, but here, the coupling effects are analyzed.

The validation process consists in comparing the numerical results, obtained by simulating the loads in a 2D axisymmetric analysis through the ANSYS software, with the analytical solutions of the problems.

CASE 1. Elastostatics

The first case of study involves the elastostatic equations that were seen in appendix D.
As previously mentioned, the element of study is a long hollow cylinder with constant thickness, inner radius a and outter radius b, in steady-state conditions and, with uniform pressure load applied at both, the inner and the outer surfaces (p_i and p_o, respectively). This is known in literature as the Lamé theory or the Thick-walled Cylinder case, where a portion of the cylinder remote from the ends is analyzed [32][12].
In this symmetric problem, the stresses and strains only vary radially, however, longitudinal stress and strain remain constant along the wall of the cylinder.

The material selected for the cylinder in this problem has been the 6061-T6 Aluminium alloy. The properties of the alloy are listed below [33].

$$E = 69.04\ GPa \qquad \lambda = 155.30\ W/mK$$
$$\nu = 0.33 \qquad \alpha = 2.278 \times 10^{-5}\ K^{-1}$$

Analytical solution

The Lamé equations for any pressure conditions at any radius r are presented below [12].

$$\sigma_{rr} = C_1 - \frac{C_2}{r^2} \tag{F.1}$$

$$\sigma_{\theta\theta} = C_1 + \frac{C_2}{r^2} \tag{F.2}$$

Given the following boundary conditions [32]:

$$\begin{aligned} r = a: \quad & \sigma_{rr} = -p_i \\ r = b: \quad & \sigma_{rr} = -p_o \end{aligned} \tag{F.3}$$

one obtains the coefficients C_1 and C_2 by substituting equations (F.33) in (F.1) and solving the system of equations.

$$C_1 = \frac{a^2 p_i - b^2 p_o}{b^2 - a^2} \qquad C_2 = \frac{(p_i - p_o)a^2 b^2}{b^2 - a^2} \tag{F.4}$$

Because the length of the cylinder has been considered to be much larger than its radius, the problem can be approached like a plane-stress case, since the nearby material of a cross-section of the cylinder remote from the ends constrains the strains associated with the longitudinal direction.

Therefore, $\varepsilon_{zz} \approx 0$ and, the solutions in terms of stress and strain is presented below.

$$\sigma_{rr} = \frac{a^2 p_i - b^2 p_o}{b^2 - a^2} - \frac{(p_i - p_o)a^2 b^2}{r^2(b^2 - a^2)} \tag{F.5}$$

$$\sigma_{\theta\theta} = \frac{a^2 p_i - b^2 p_o}{b^2 - a^2} + \frac{(p_i - p_o)a^2 b^2}{r^2(b^2 - a^2)} \tag{F.6}$$

$$\sigma_{zz} = 2\nu \frac{(a^2 p_i - b^2 p_o)}{b^2 - a^2} \tag{F.7}$$

$$\varepsilon_{rr} = \frac{1}{E}\left[\sigma_{rr} - \nu(\sigma_{\theta\theta} + \sigma_{zz})\right] \tag{F.8}$$

$$\varepsilon_{\theta\theta} = \frac{1}{E}\left[\sigma_{\theta\theta} - \nu(\sigma_{rr} + \sigma_{zz})\right] \tag{F.9}$$

Note that the stresses on an element at any point on the cylinder wall are principal stresses, therefore, the maximum shear stress at any point will be given by

$$\tau_{max} = \frac{\sigma_1 - \sigma_3}{2} \tag{F.10}$$

Moreover, the change of diameter and length of the cylinder at any radius r are given by

$$\Delta D = 2r\varepsilon_{\theta\theta} \tag{F.11}$$

$$\Delta L = L\varepsilon_{zz} \tag{F.12}$$

Numerical analysis

The numerical analysis of the first case has been done, as previously mentioned, by discretizing a portion of a cylinder into several finite elements and solving the finite element method (FEM) through the ANSYS software.

The first step to define is the type of analysis to be performed, in this case a static structural analysis. Next to be defined is the geometry, which has been defined as the cross-section of a cylinder (see figure D.3) with dimensions

$$a = 35\ mm \text{ (inner radius)}$$

$$b = 40\ mm \text{ (outer radius)}$$

$$L = 0.25\ m \text{ (length)}$$

The next step is to mesh the geometry defined, i.e. to divide the geometry into several finite elements, defining the number of elements introduced and the type of elements used. In this case, quadrilateral elements have been employed and the total number of elements used are 2500, resulting from the partition of the wall along the radial direction into 50 divisions and, along the axial direction into 50 divisions as well (see figure F.1).

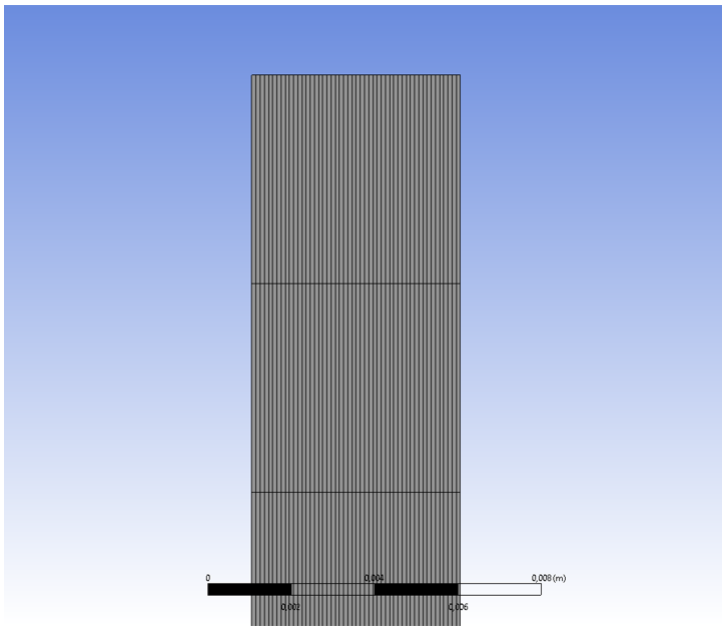

Figure F.1: Image of the mesh employed in the numerical analysis of cases 1, 2 and 3 for the validation process. Note that only a portion of the mesh is showed for clarity and visualization purposes.

Once the geometry has been defined and meshed, the following step is the definition of its boundary conditions (BC). A total of four boundary conditions have been applied, two Dirichlet BC and two Neumann BC, and are listed below.

- Internal pressure. A constant and homogeneous pressure of $p_i = 2\ MPa$ has been applied over the internal surface.
- External pressure. A constant and homogeneous pressure of $p_o = 101325\ Pa$ (i.e., 1 atm) has been applied over the external surface.
- Friction-less support. The bottom surface has been restricted in the axial direction while left free from displacements and deformations in the radial direction.
- Prescribed displacement. The axial displacement of the top surface has been set to 0 m while leaving free the radial direction for displacements and deformations. Note that those last BC make reference to the plane-strain approach mentioned previously.

Validation

Finally, the results obtained from both, the analytical and numerical analysis have been plot and compared in figures F.2 to F.7, with a maximum relative error of 0.02%.

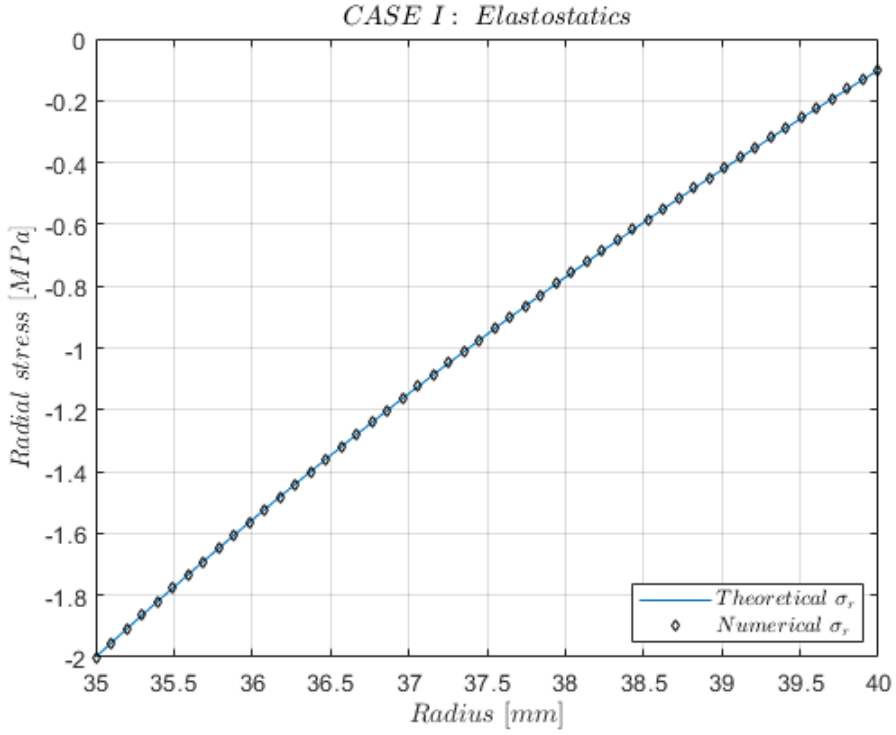

Figure F.2: Radial stress numerical vs analytical results as a function of the wall thickness.

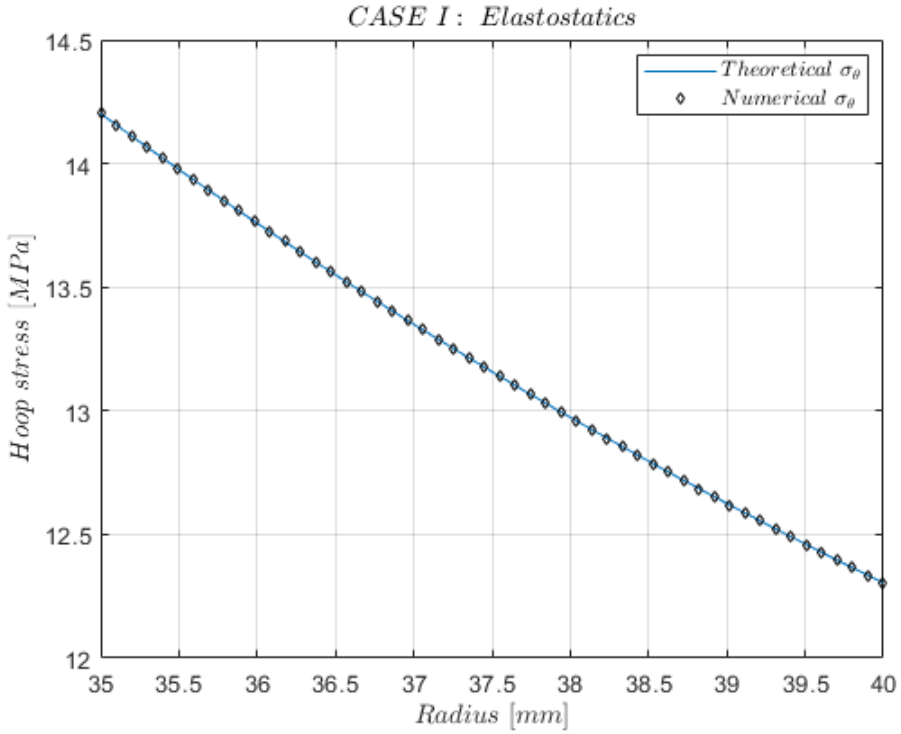

Figure F.3: Hoop stress numerical vs analytical results as a function of the wall thickness.

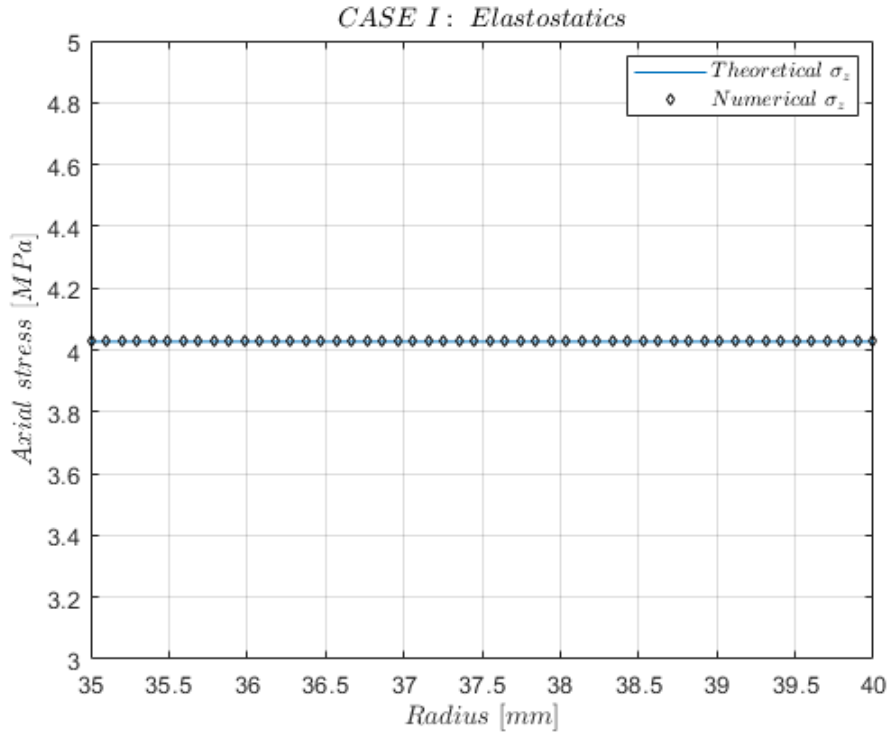

Figure F.4: Axial stress numerical vs analytical results as a function of the wall thickness.

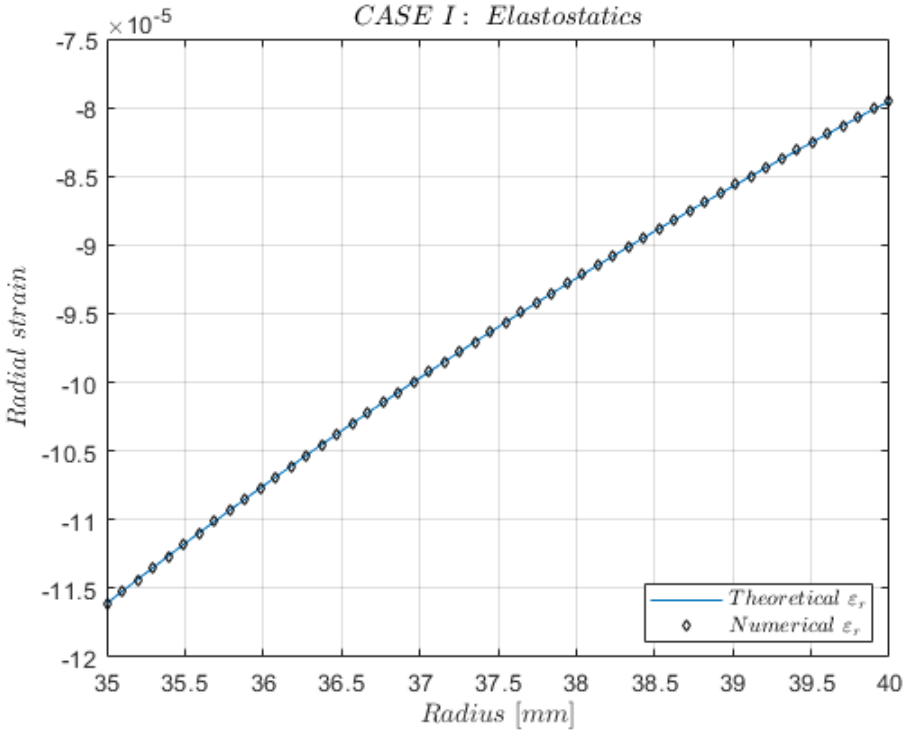

Figure F.5: Radial strain numerical vs analytical results as a function of the wall thickness.

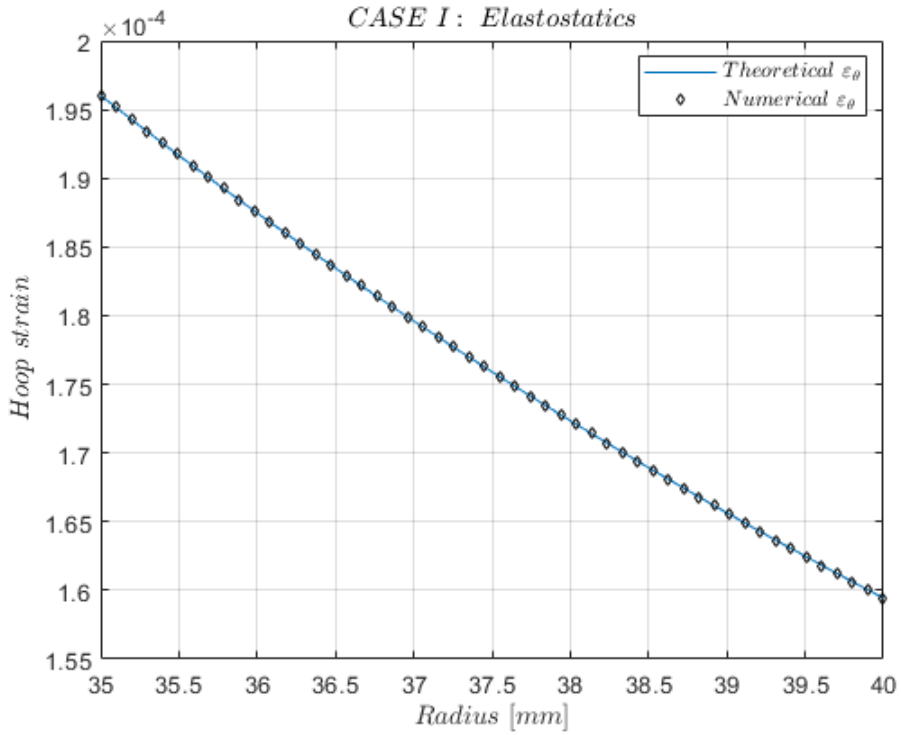

Figure F.6: Hoop strain numerical vs analytical results as a function of the wall thickness.

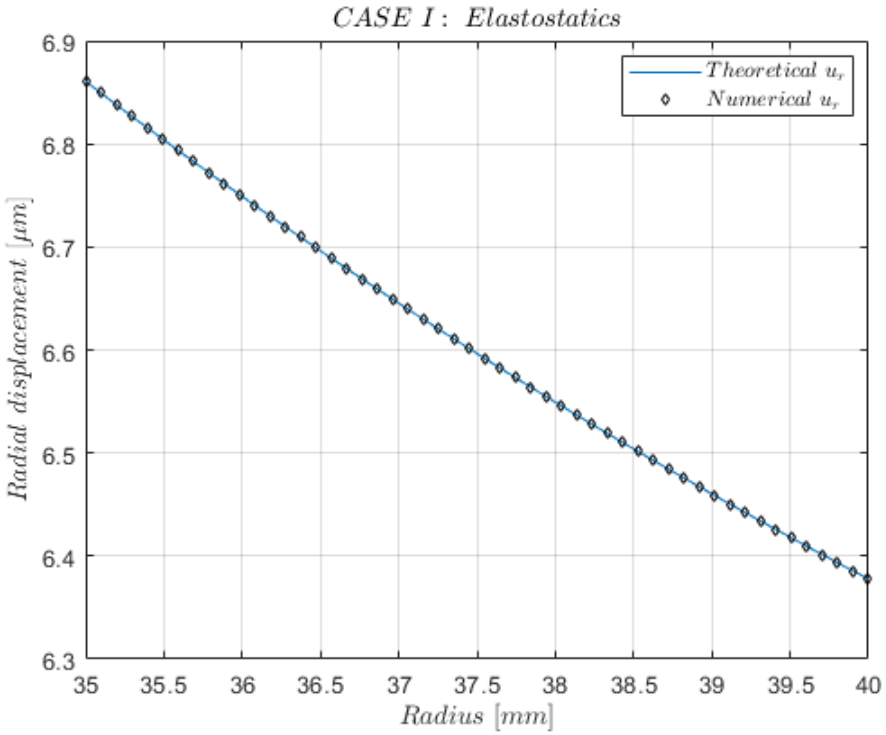

Figure F.7: Radial displacement numerical vs analytical results as a function of the wall thickness.

CASE 2. Convective heat transfer

The second case of study involves heat transfer along the walls of the cylinder. In this case, the inner surface is subjected to a forced convection (at low Mach number) and the outer surface is subjected to a natural convection. The cylinder is at steady-state conditions and, since the portion of cylinder studied is far from the edges of the cylinder, the heat flux can be considered to vary radially. Constant thermal properties are also considered and, no internal heat sources are present.

The fluids selected for this problem and their respective thermophysical properties are the following:

Inside the cylinder, steam at $T_i = 500\ °C$ and $p_i = 2.0\ MPa$ (same pressure as case 1) [34].

$$\mu_i = 2.8605 \times 10^{-5}\ kg/ms \qquad \lambda_i = 0.068127\ W/mK$$
$$c_{p_i} = 2206.2\ J/kgK \qquad \rho_i = 5.6921\ kg/m^3$$

Outside the cylinder, dry air at $T_o = 20\ °C$ and $p_o = 101325\ Pa$ (same pressure as case 1).

$$\mu_o = 1.813 \times 10^{-6}\ kg/ms \qquad \lambda_o = 0.0257\ W/mK$$
$$c_{p_o} = 1006.021\ J/kgK \qquad \rho_o = 1.204\ kg/m^3$$
$$\beta_o = 3.411 \times 10^{-3}\ K^{-1}$$

Analytical solution

The equations of temperature and heat flux distribution at any radius r of the cylinder are given by [22][23]

$$T = C_1 ln(r) + C_2 \tag{F.13}$$
$$\dot{q}_r = -\lambda \frac{C_1}{r} \tag{F.14}$$

Given the following boundary conditions:

$$r = a \quad \begin{cases} T = T_{w_i} \\ \dot{q}_r = h_i(T_i - T_{w_i}) \end{cases} \qquad r = b \quad \begin{cases} T = T_{w_o} \\ \dot{q}_r = h_o(T_{w_o} - T_o) \end{cases} \tag{F.15}$$

where T_{w_i} is the wall temperature of the inner surface, T_{w_o} is the wall temperature of the outer surface, T_i is the temperature of the internal gas, T_o is the temperature of the outer gas, h_i is the convection heat transfer coefficient of the internal gas and, h_o is the convection heat transfer coefficient of the outer gas.

Then, one obtains the coefficients C_1 and C_2 by substituting equations (F.15) in (F.13) and (F.14) and, solving the system of equations.

$$C_1 = \frac{T_o - T_i}{\frac{\lambda}{bh_o} + ln(b) + \frac{\lambda}{ah_i} - ln(a)} \qquad C_2 = \frac{T_o\left(\frac{\lambda}{bh_o} + ln(b)\right) + T_i\left(\frac{\lambda}{ah_i} - ln(a)\right)}{\frac{\lambda}{bh_o} + ln(b) + \frac{\lambda}{ah_i} - ln(a)} \tag{F.16}$$

Therefore, the solution in terms of temperature and radial heat flux per unit surface at any radius r of the cylinder are given by

$$T = \frac{(T_o - T_i)}{\frac{\lambda}{bh_o} + ln(b) + \frac{\lambda}{ah_i} - ln(a)} ln(r) + \frac{T_o\left(\frac{\lambda}{bh_o} + ln(b)\right) + T_i\left(\frac{\lambda}{ah_i} - ln(a)\right)}{\frac{\lambda}{bh_o} + ln(b) + \frac{\lambda}{ah_i} - ln(a)} \tag{F.17}$$

$$\dot{q}_r = -\frac{\lambda}{r} \frac{(T_o - T_i)}{\left(\frac{\lambda}{bh_o} + ln(b) + \frac{\lambda}{ah_i} - ln(a)\right)} \tag{F.18}$$

Note that both convective processes have the same expression in terms of heat flux (see boundary conditions), however, the heat transfer coefficient differentiates between a forced and a natural convection, since both coefficients will be obtained through experimental expressions [35].

For forced convection at low Mach number, the heat transfer coefficient can be found by computing several adimentional groups such as the Reynolds number (Re), the Prandtl number (Pr) and, the mean Nusselt number ($\overline{Nu}$).

$$Pr = \frac{\mu_i c_{p_i}}{\lambda_i} \tag{F.19}$$

$$Re = \frac{\rho_i \bar{v} D}{\mu_i} \tag{F.20}$$

$$\overline{Nu} = C Re^m Pr^n K \tag{F.21}$$

$$h_i = \frac{\overline{Nu}\lambda_i}{D} \tag{F.22}$$

where C, m, n and K are experimental parameters, D is the hydraulic diameter and, $\bar{v}$ is the mean inner fluid velocity. The expressions of which are

$$D = 4\frac{S}{P} \qquad \bar{v} = \frac{\dot{m}}{\rho_i S} \tag{F.23}$$

where S is the inner cross sectional area, P is the inner wet perimeter and, $\dot{m}$ is the mass flow rate of the inner fluid.

For the natural/free convection of the exterior surface, the heat transfer coefficient can be found also through adimentional groups, but in this case are the Grashof number (Gr), the Prandtl number (Pr), the Rayleigh number (Ra) and, the mean Nusselt number ($\overline{Nu}$).

$$Gr = \frac{g\beta_o \rho_o^2 |T_{w_o} - T_o| X^3}{\mu_o^2} \tag{F.24}$$

$$Pr = \frac{\mu_o c_{p_o}}{\lambda_o} \tag{F.25}$$

$$Ra = GrPr \tag{F.26}$$

$$\overline{Nu} = C Ra^n K \tag{F.27}$$

$$h_o = \frac{\overline{Nu}\lambda_o}{X} \tag{F.28}$$

where C, n and K are experimental parameters and, X a reference distance (in the case of natural convection with a vertical cylinder $X = L$).

Numerical analysis

The procedure followed to perform the numerical analysis of the second case is similar to the one followed in the elastostatic problem. In this case though, the analysis performed has been a steady-state thermal.
The geometry employed in this analysis is exactly the same as in the previous case, and so is the mesh. Regarding the boundary conditions, the following convective flows have been applied:

- Forced convection. A forced convection of steam at 500 $°C$ with a film coefficient of $h_i = 3455.6\ W/m^2K$ has been applied over the inner surface of the cylinder.
- Natural or free convection. A natural convection of dry air at 20 $°C$ with a film coefficient of $h_o = 10.8061\ W/m^2K$ has been applied over the outer surface of the cylinder.

Validation

The results obtained from the two approaches, the analytical and the numerical, are presented in figures F.8 and F.9, with a maximum relative error of 0.06%.

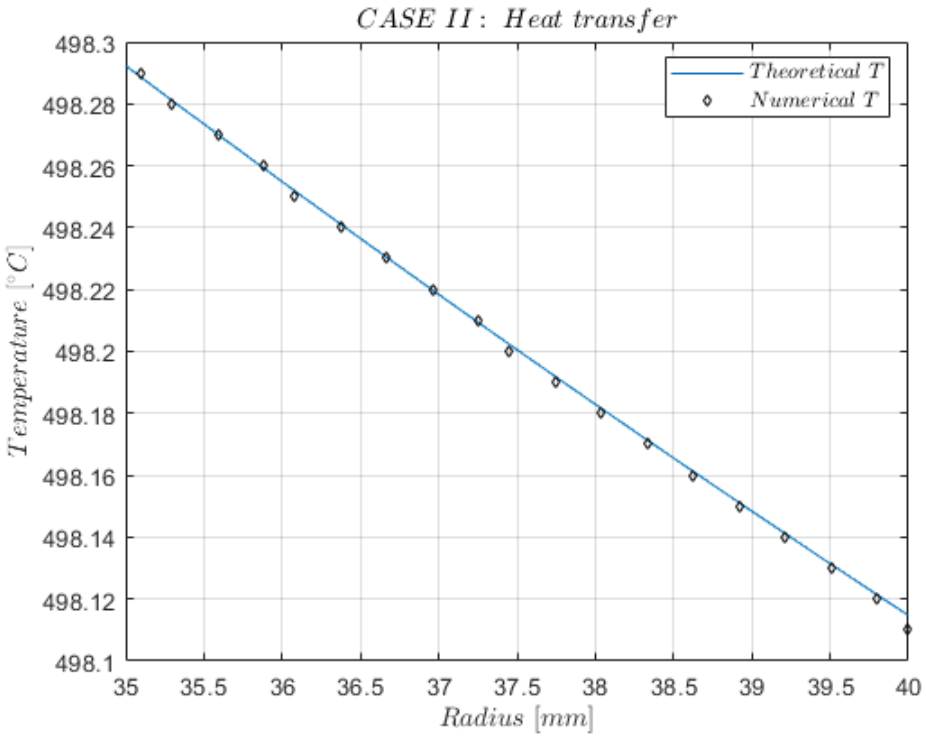

Figure F.8: Temperature numerical vs analytical results as a function of the wall thickness.

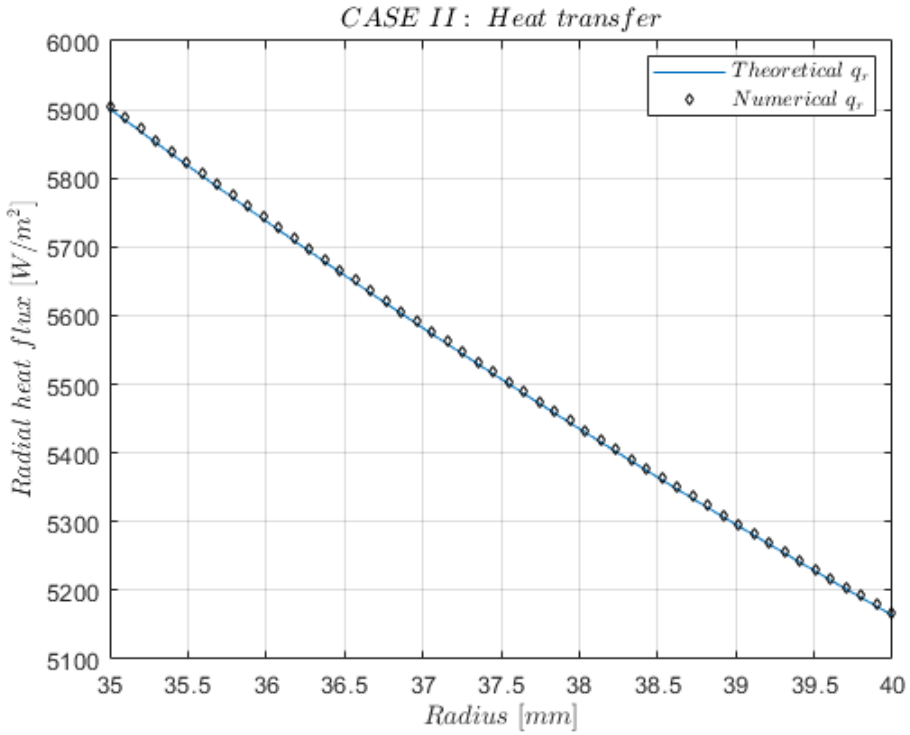

Figure F.9: Radial heat flux numerical vs analytical results as a function of the wall thickness.

CASE 3. Thermoeslasticity

The third case of study is a thermoelastic analysis of the same cylinder of cases 1 and 2. Here, the mechanical loads derived from the pressures applied in case 1 and, the thermal loads derived from the convection of case 2 are coupled to account for both effects. The same assumptions, materials and fluids of previous cases are applied as well.

Analytical solution

The strain equations that relate mechanical and thermal loads are presented below [28][30]

$$\varepsilon_{rr} = \frac{1}{E}\left[\sigma_{rr} - \nu\left(\sigma_{\theta\theta} + \sigma_{zz}\right)\right] + \alpha\Delta T \tag{F.29}$$

$$\varepsilon_{\theta\theta} = \frac{1}{E}\left[\sigma_{\theta\theta} - \nu\left(\sigma_{rr} + \sigma_{zz}\right)\right] + \alpha\Delta T \tag{F.30}$$

$$\varepsilon_{zz} = \frac{1}{E}\left[\sigma_{zz} - \nu\left(\sigma_{rr} + \sigma_{\theta\theta}\right)\right] + \alpha\Delta T \tag{F.31}$$

where α is the thermal expansion coefficient and ΔT the change in temperature with respect to a reference temperature (T_{ref}).

From reference [32], the expression of the radial stress before applying any boundary condition is the following.

$$\sigma_{rr} = \frac{E}{1+\nu}\left(-\frac{(1+\nu)}{(1-\nu)}\frac{1}{r^2}\int_a^r \alpha\Delta T r\, dr + \frac{C_3}{1-2\nu} - \frac{C_4}{r^2} + \frac{\nu}{1-2\nu}\varepsilon_{zz}\right) \tag{F.32}$$

By applying the boundary conditions of a state with thermal load only

$$\begin{aligned} r = a: &\quad \sigma_{rr} = 0 \\ r = b: &\quad \sigma_{rr} = 0 \end{aligned} \tag{F.33}$$

one obtains the integration coefficients C_3 and C_4

$$C_3 = \frac{(1+\nu)(1-2\nu)}{(1-\nu)} \frac{1}{(b^2-a^2)} \int_a^b \alpha \Delta T r \, dr - \nu \varepsilon_{zz} \tag{F.34}$$

$$C_4 = \frac{(1+\nu)}{(1-\nu)} \frac{a^2}{(b^2-a^2)} \int_a^b \alpha \Delta T r \, dr \tag{F.35}$$

With those coefficients, references [32] and [36] present the general expressions of the principal stresses for a thermal load only condition.

$$\sigma_{rr} = \frac{E}{1-\nu} \left(-\frac{1}{r^2} \int_a^r \alpha \Delta T r \, dr + \frac{r^2-a^2}{r^2(b^2-a^2)} \int_a^b \alpha \Delta T r \, dr \right) \tag{F.36}$$

$$\sigma_{\theta\theta} = \frac{E}{1-\nu} \left(\frac{1}{r^2} \int_a^r \alpha \Delta T r \, dr + \frac{r^2+a^2}{r^2(b^2-a^2)} \int_a^b \alpha \Delta T r \, dr - \alpha \Delta T \right) \tag{F.37}$$

$$\sigma_{zz} = \frac{E}{1-\nu} \left(\frac{2}{b^2-a^2} \int_a^b \alpha \Delta T r \, dr - \alpha \Delta T \right) \tag{F.38}$$

By substituting the temperature distribution expression obtained in case 2,

$$\Delta T = T - T_{ref} = C_1 ln(r) + C_2 - T_{ref} \tag{F.39}$$

the thermal stresses generated during the steady-state convection are found.

$$\sigma_{rr} = \frac{\alpha E}{2(1-\nu)} C_1 \left[\frac{a^2(b^2-r^2)}{r^2(b^2-a^2)} \left(ln(a) - \frac{1}{2} \right) + \frac{b^2(r^2-a^2)}{r^2(b^2-a^2)} \left(ln(b) - \frac{1}{2} \right) - ln(r) + \frac{1}{2} \right] \tag{F.40}$$

$$\sigma_{\theta\theta} = \frac{\alpha E}{2(1-\nu)} C_1 \left[-\frac{a^2(b^2+r^2)}{r^2(b^2-a^2)} \left(ln(a) - \frac{1}{2} \right) + \frac{b^2(r^2+a^2)}{r^2(b^2-a^2)} \left(ln(b) - \frac{1}{2} \right) - ln(r) - \frac{1}{2} \right] \tag{F.41}$$

$$\sigma_{zz} = -\frac{\alpha E}{1-\nu} C_1 \left[\frac{a^2(ln(a) - \frac{1}{2}) - b^2(ln(b) - \frac{1}{2})}{b^2-a^2} + ln(r) \right] \tag{F.42}$$

In order to obtain the total stresses of the cylinder, the mechanical stresses of case 1 are superposed to the thermal stresses just found.

$$\sigma_{rr} = \sigma_{rr}^{mechanical} + \sigma_{rr}^{thermal} \tag{F.43}$$

$$\sigma_{\theta\theta} = \sigma_{\theta\theta}^{mechanical} + \sigma_{\theta\theta}^{thermal} \tag{F.44}$$

$$\sigma_{zz} = \sigma_{zz}^{mechanical} + \sigma_{zz}^{thermal} \tag{F.45}$$

Numerical analysis

The numerical analysis of this case has been also carried out with the ANSYS software proceeding as follows: 1) A steady-state thermal analysis,identical as in case 2, has been simulated. 2) Next, a steady-state structural analysis with the results of the thermal analysis loaded, i.e. the temperature distribution, has been carried out to account for both, mechanical and thermal loads.

The case has also been simulated in a 2D axysimmetric geometry with the same geometry, mesh and boundary conditions as cases 1 and 2.

Validation

The results obtained from the analytical and numerical methods are compared in the figures below.

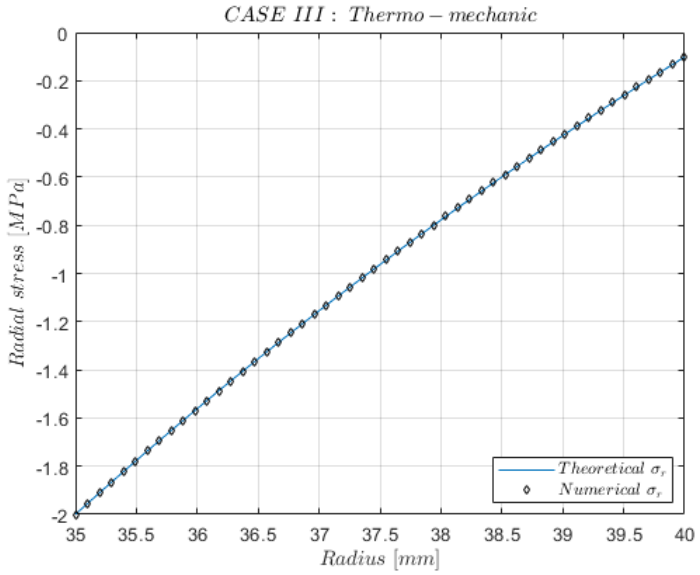

Figure F.10: Radial stress numerical vs analytical results as a function of the wall thickness.

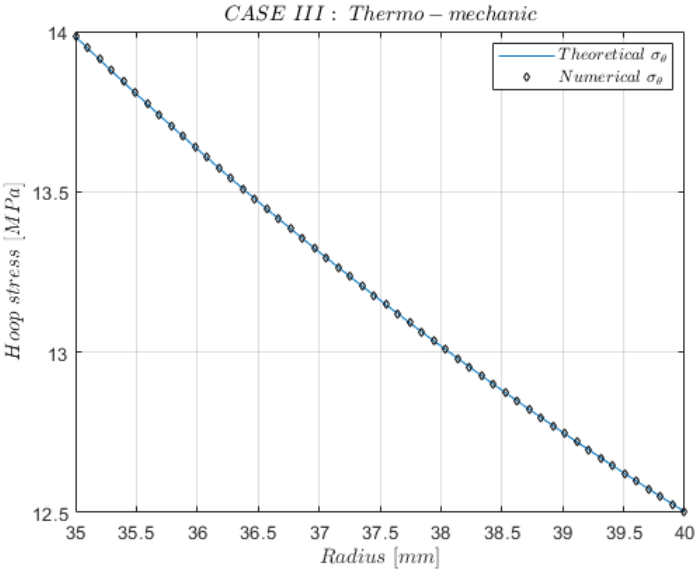

Figure F.11: Hoop stress numerical vs analytical results as a function of the wall thickness.

Appendix G

Thermomechanical results for maximum chamber pressure instant

In this appendix, the results at maximum pressure instant of the separate effects of the mechanical and thermal loads from the seventh analysis are presented.

Note that stresses generated by thermal loads are showed only at the nozzle, since the rest of the structure stays at room temperature and, therefore, no material expansion is produced there.

Stresses from thermal loads

Equivalent Stress (Von Mises)

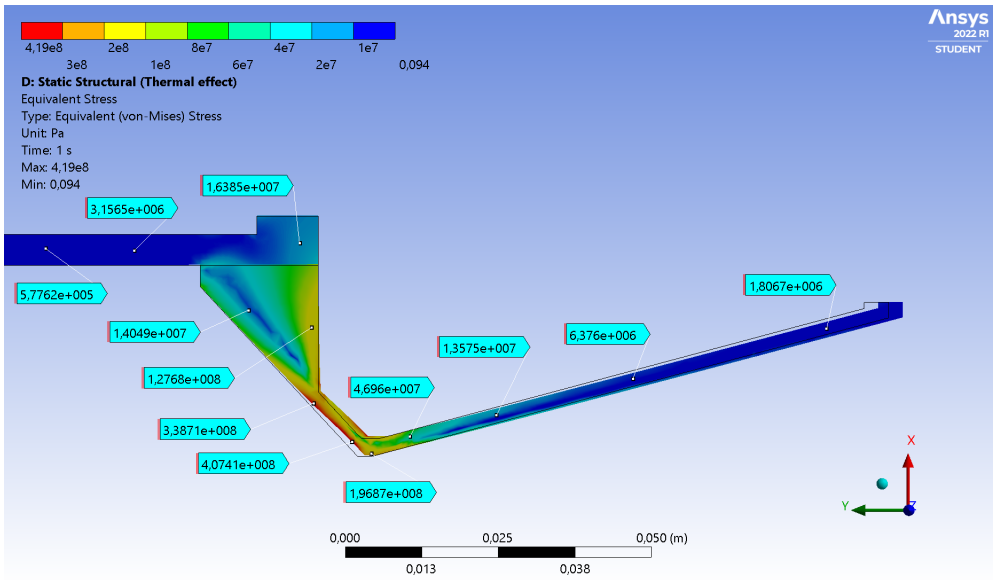

Figure G.1: Zoom-in view of the bottom end's Von Mises stress distribution (Analysis 7). Scale factor: 15.

Radial Stress

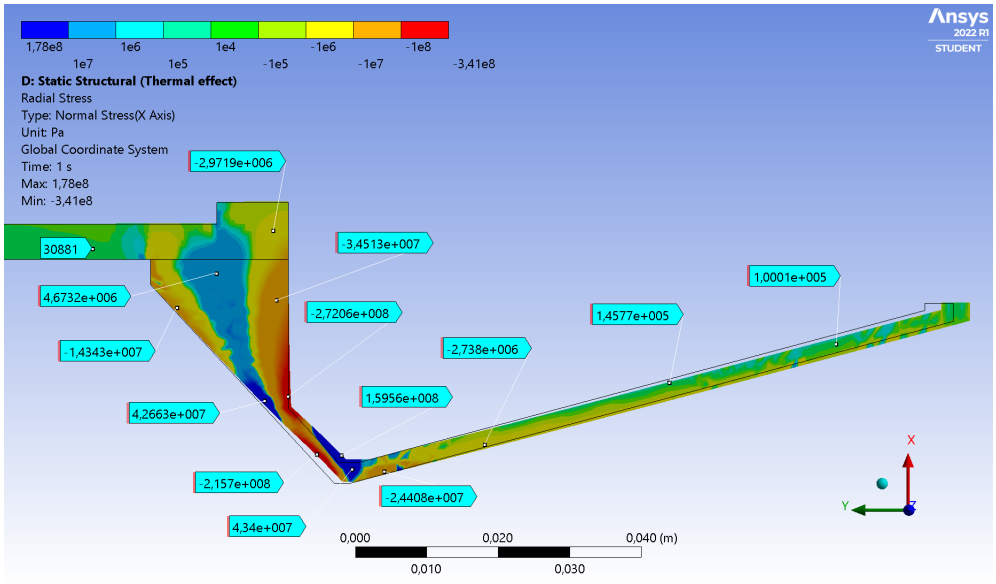

Figure G.2: Zoom-in view of the bottom end's radial stress distribution (Analysis 7). Scale factor: 15.

Hoop Stress

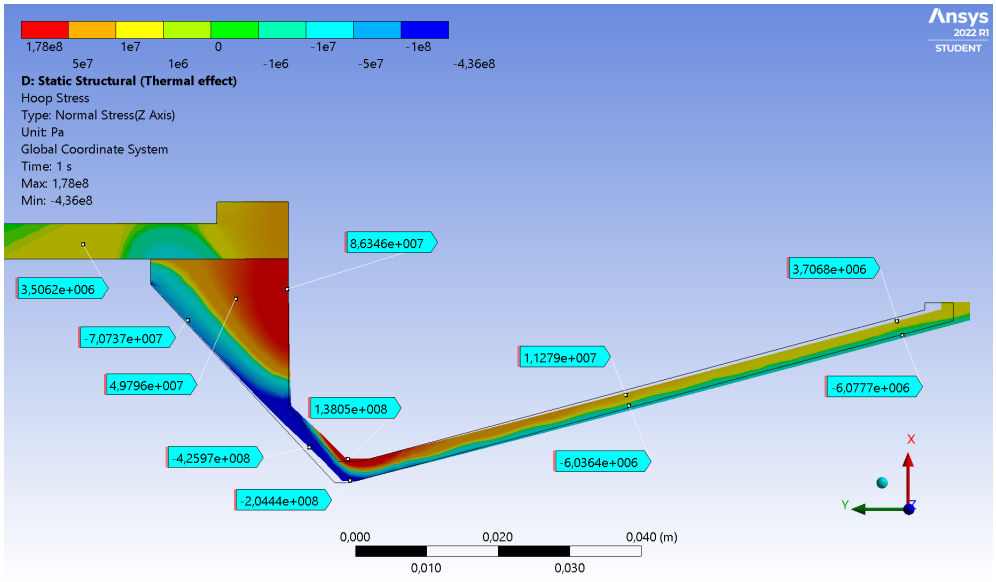

Figure G.3: Zoom-in view of the bottom end's hoop stress distribution (Analysis 7). Scale factor: 15.

Axial Stress

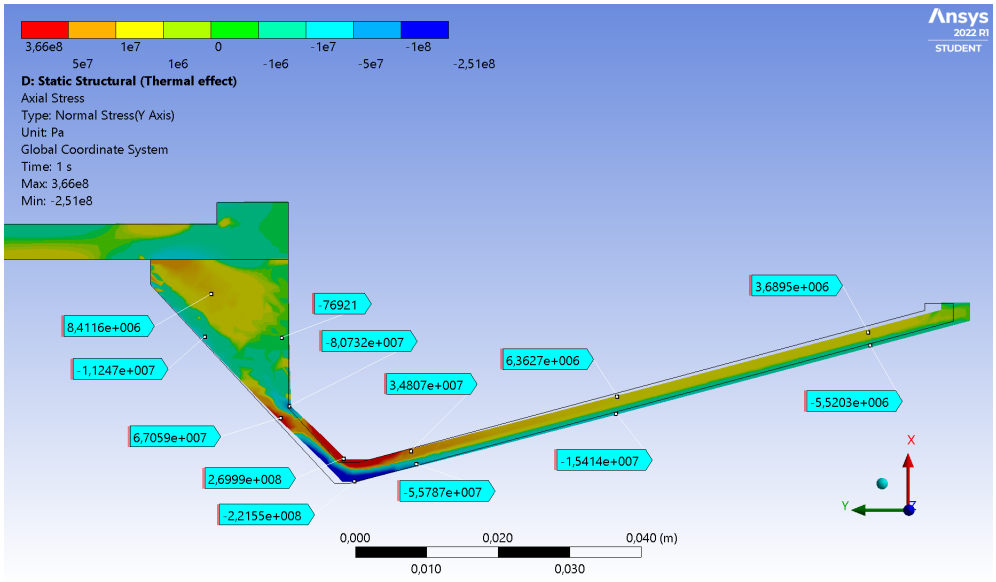

Figure G.4: Zoom-in view of the bottom end's axial stress distribution (Analysis 7). Scale factor: 15.

Stresses from mechanical loads

Equivalent Stress (Von Mises)

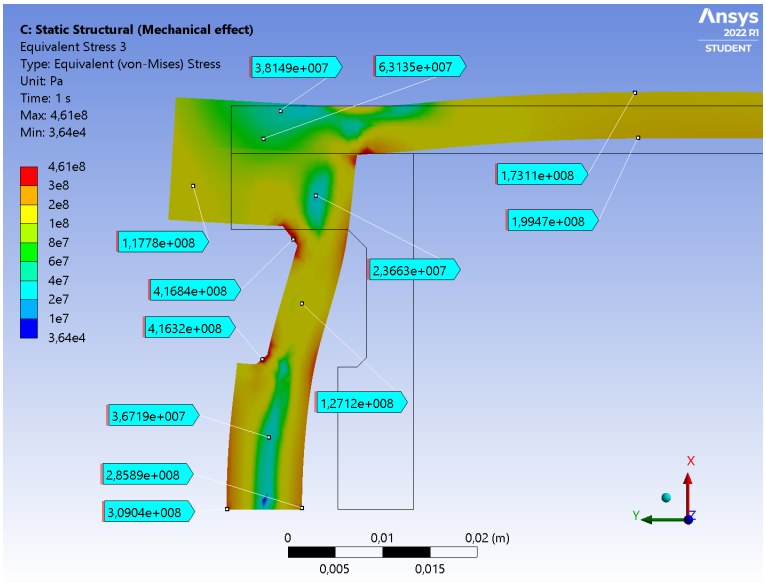

Figure G.5: Zoom-in view of the top end's Von Mises stress distribution (Analysis 7). Scale factor: 15.

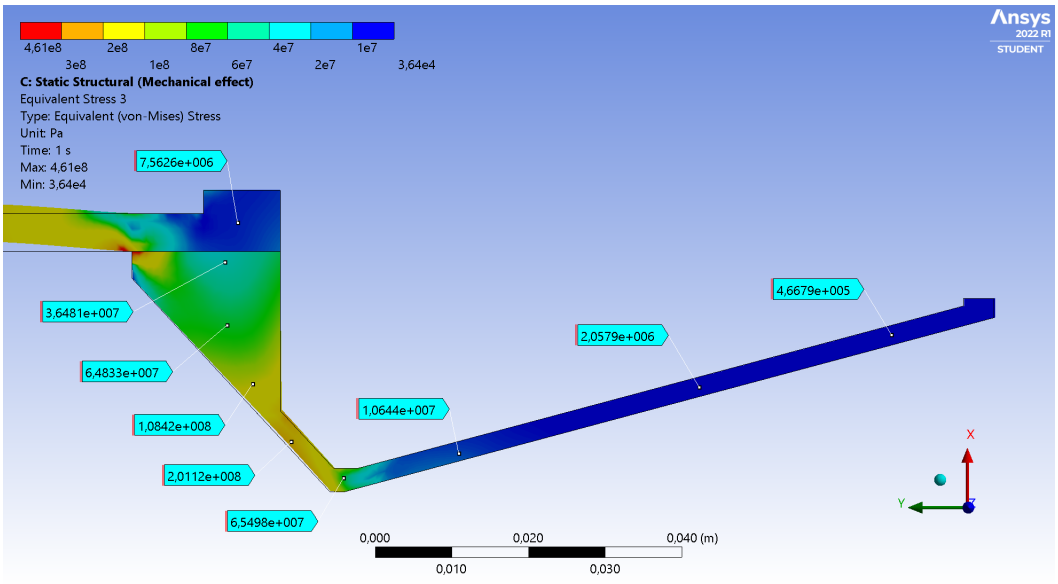

Figure G.6: Zoom-in view of the bottom end's Von Mises stress distribution (Analysis 7). Scale factor: 15.

Radial Stress

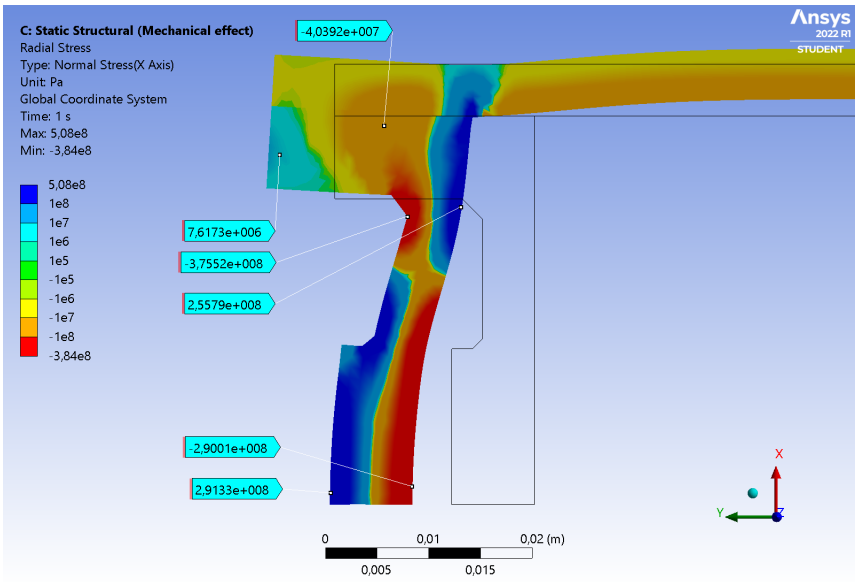

Figure G.7: Zoom-in view of the top end's radial stress distribution (Analysis 7). Scale factor: 15.

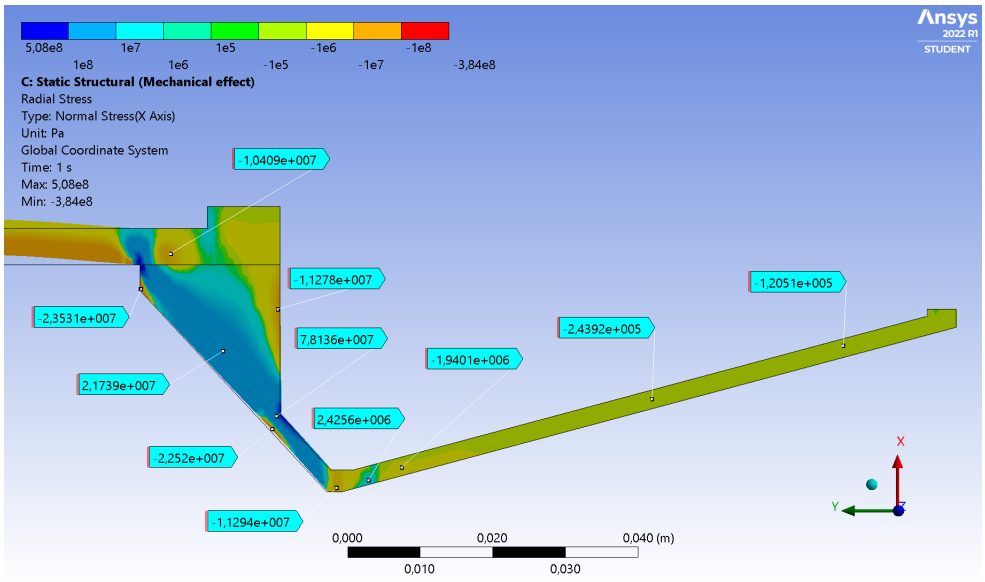

Figure G.8: Zoom-in view of the bottom end's radial stress distribution (Analysis 7). Scale factor: 15.

Hoop Stress

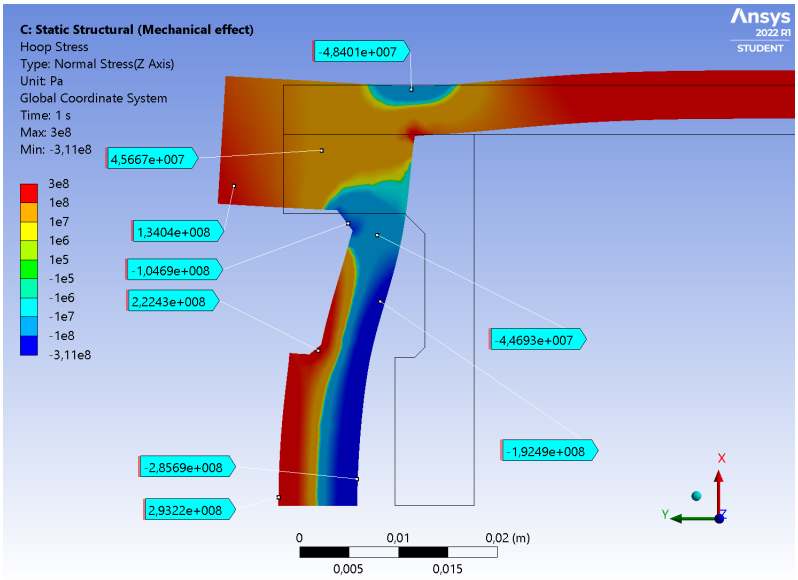

Figure G.9: Zoom-in view of the top end's hoop stress distribution (Analysis 7). Scale factor: 15.

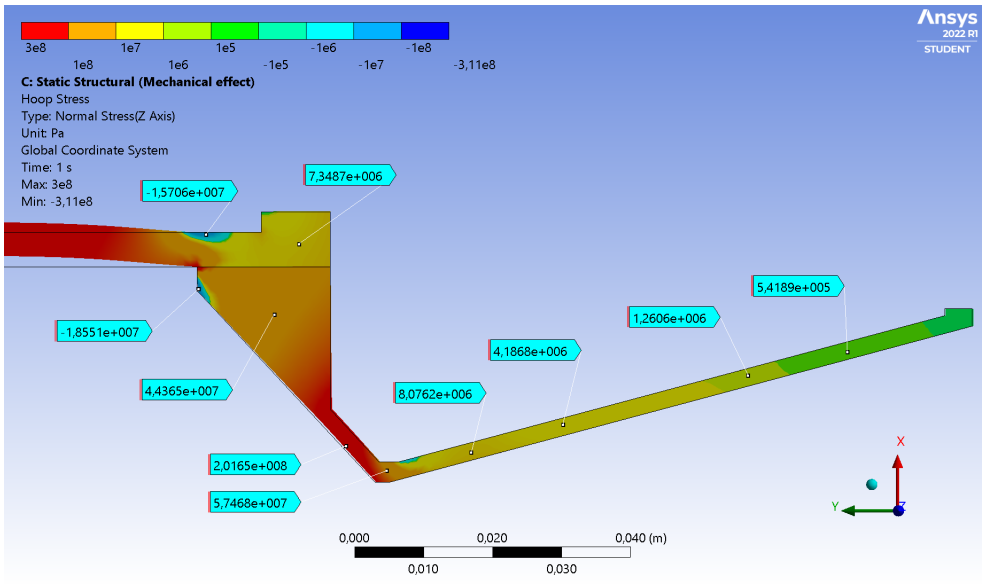

Figure G.10: Zoom-in view of the bottom end's hoop stress distribution (Analysis 7). Scale factor: 15.

Axial Stress

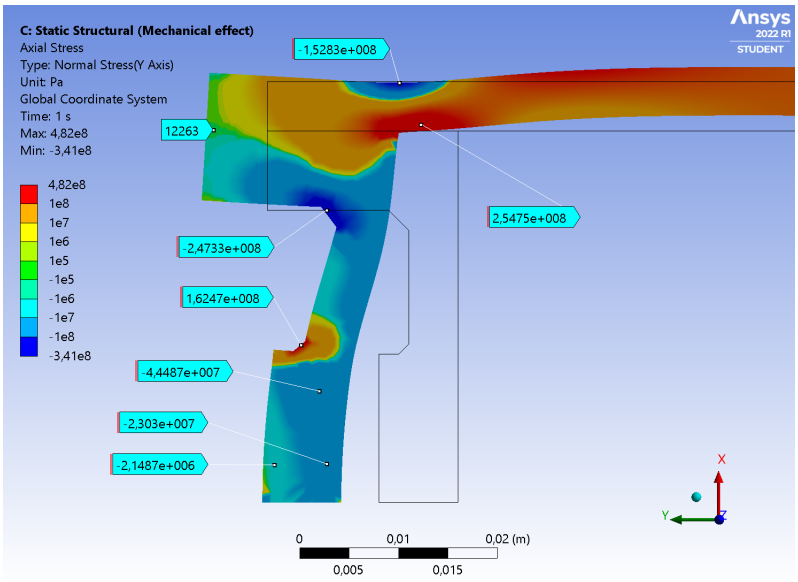

Figure G.11: Zoom-in view of the top end's axial stress distribution (Analysis 7). Scale factor: 15.

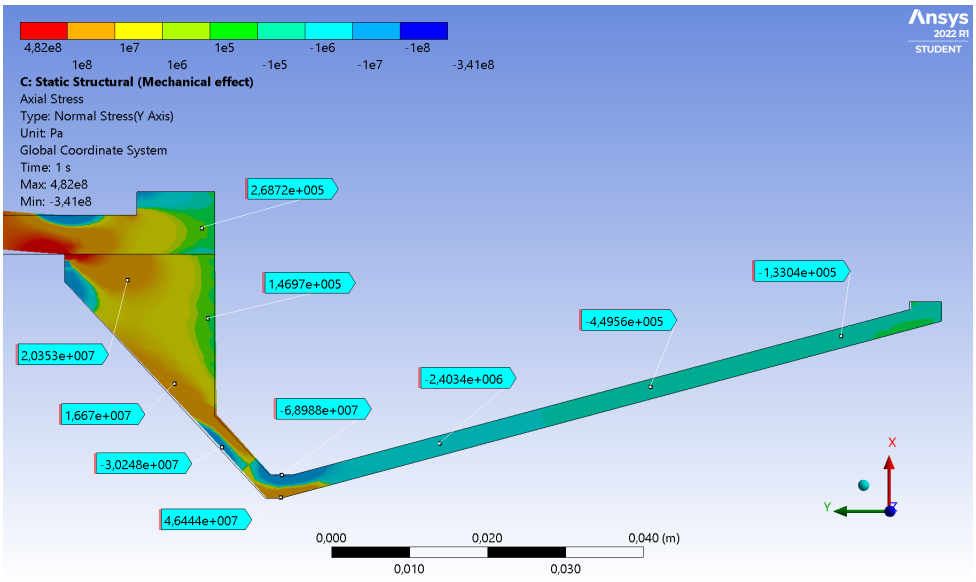

Figure G.12: Zoom-in view of the bottom end's axial stress distribution (Analysis 7). Scale factor: 15.

Appendix H

Thermomechanical results for maximum nozzle temperature instant

This appendix contains the results at the maximum nozzle temperature instant with the separate effects of the mechanical and thermal loads.

Note that only the nozzle distributions are presented, since the forward closure has already proved to withstand the most harsh conditions, which arise when the maximum chamber pressure is reached.

Stresses from thermal loads

Equivalent Stress (Von Mises)

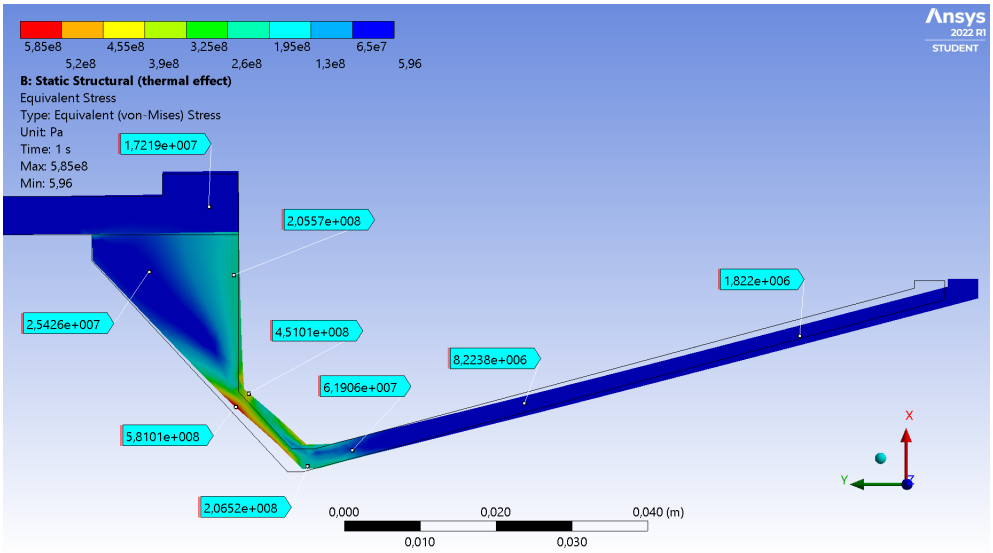

Figure H.1: Zoom-in view of the bottom end's Von Mises stress distribution (Analysis 8). Scale factor: 15.

Radial Stress

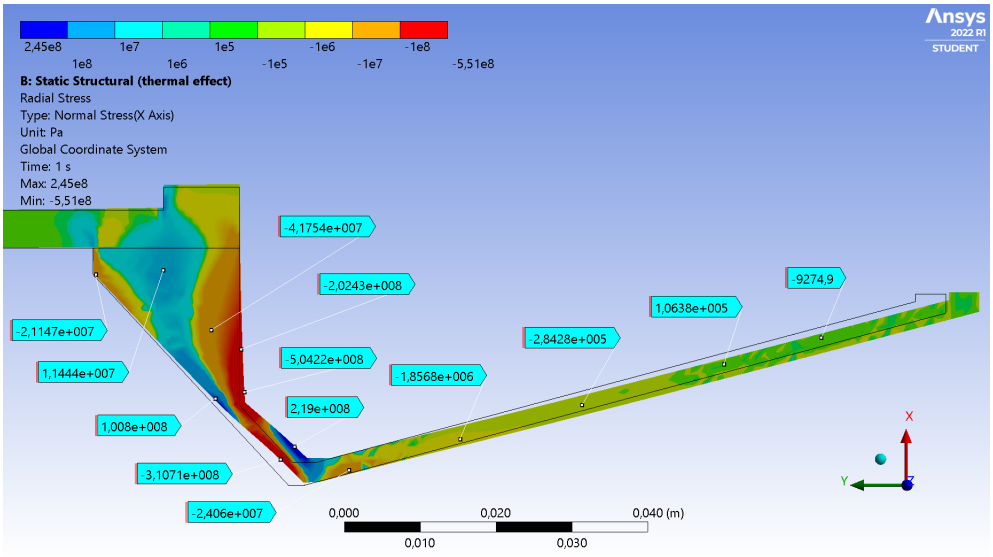

Figure H.2: Zoom-in view of the bottom end's radial stress distribution (Analysis 8). Scale factor: 15.

Hoop Stress

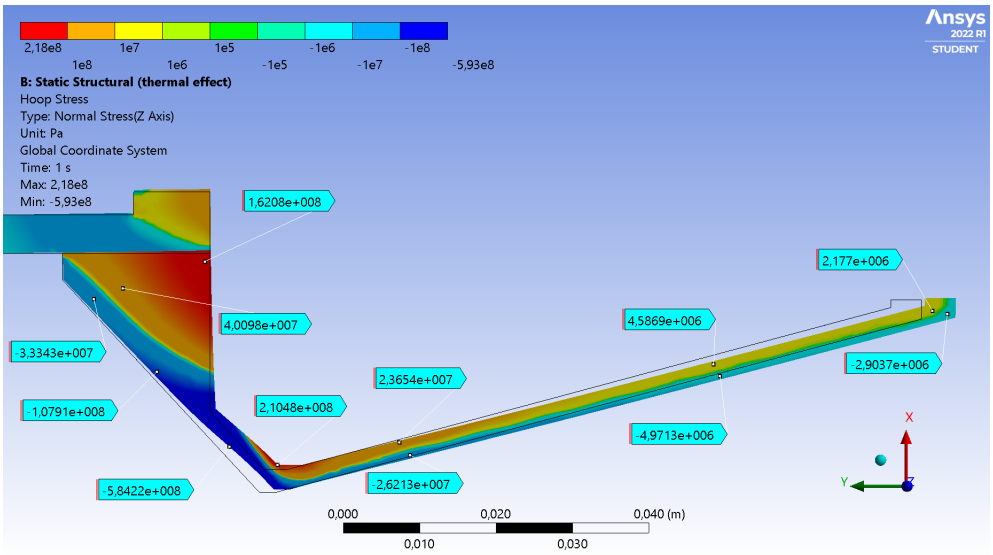

Figure H.3: Zoom-in view of the bottom end's hoop stress distribution (Analysis 8). Scale factor: 15.

Axial Stress

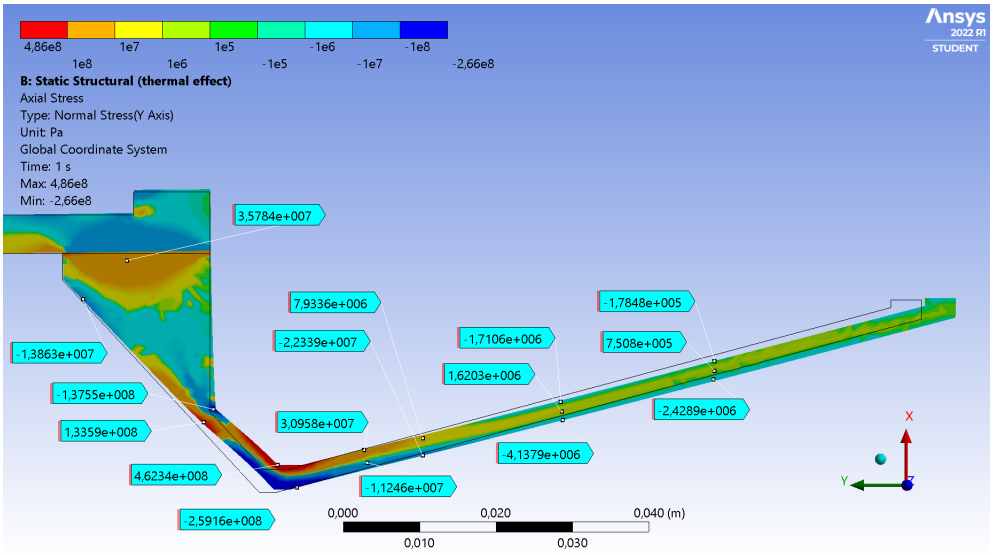

Figure H.4: Zoom-in view of the bottom end's axial stress distribution (Analysis 8). Scale factor: 15.

Stresses from mechanical loads

Equivalent Stress (Von Mises)

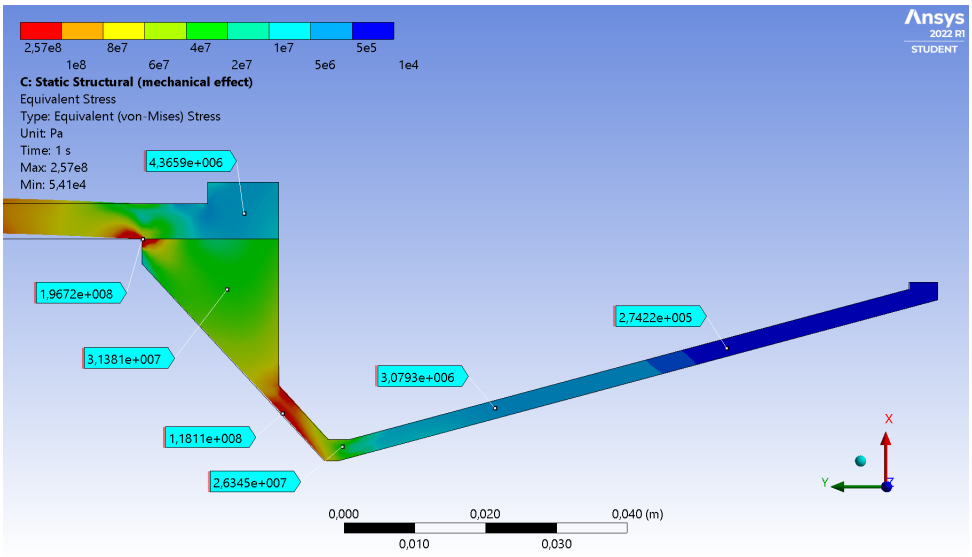

Figure H.5: Zoom-in view of the bottom end's Von Mises stress distribution (Analysis 8). Scale factor: 15.

Radial Stress

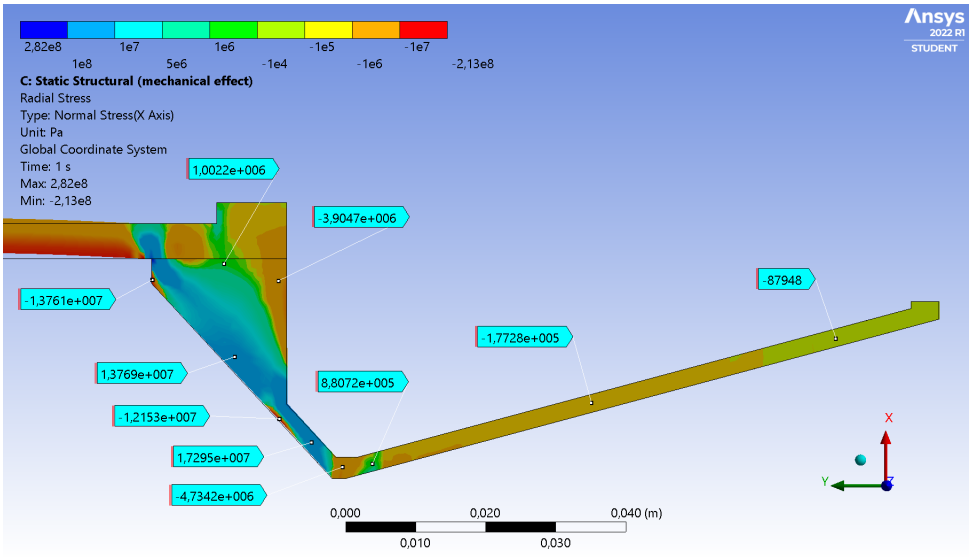

Figure H.6: Zoom-in view of the bottom end's radial stress distribution (Analysis 8). Scale factor: 15.

Hoop Stress

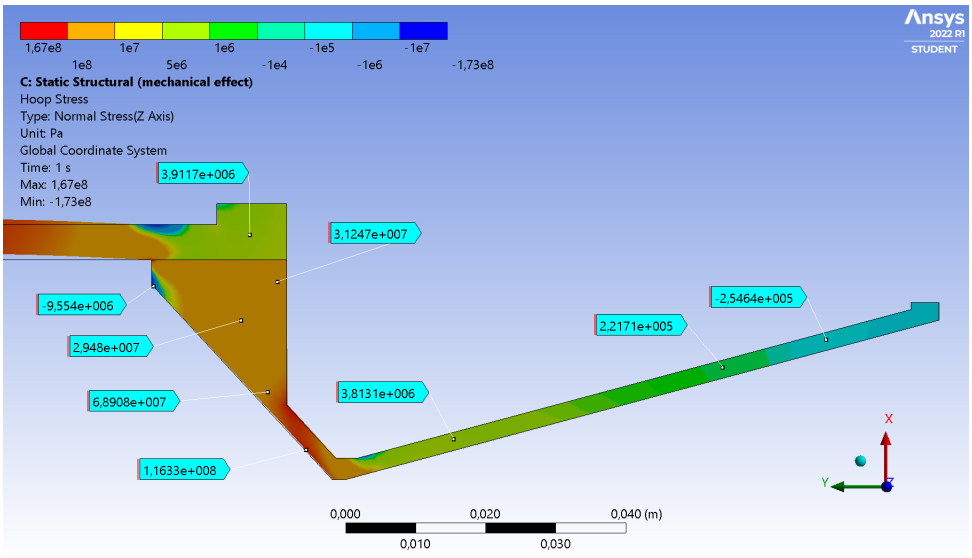

Figure H.7: Zoom-in view of the bottom end's hoop stress distribution (Analysis 8). Scale factor: 15.

Axial Stress

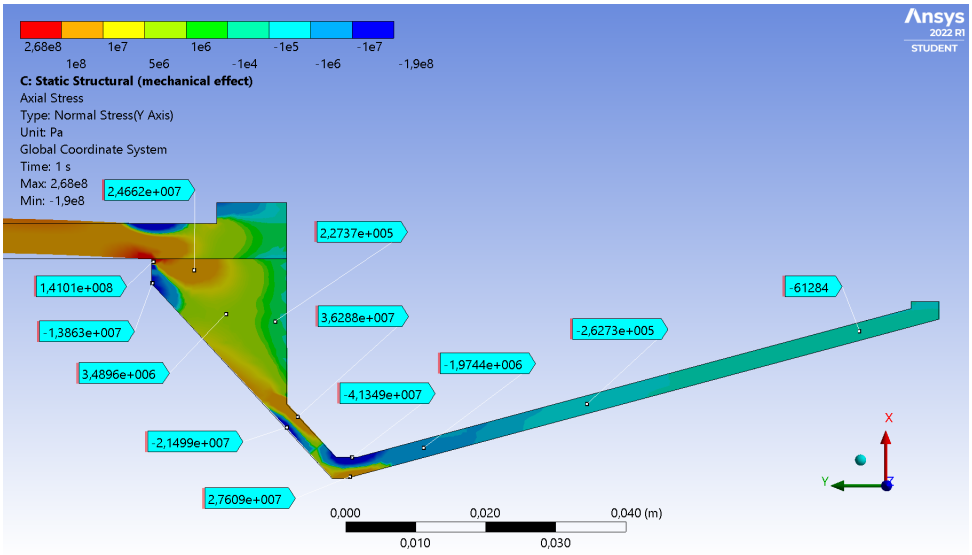

Figure H.8: Zoom-in view of the bottom end's axial stress distribution (Analysis 8). Scale factor: 15.